Mid-Century Ensemble Regional Climate Change Scenarios For the Western United States

L. Ruby Leung, Yun Qian, and Xindi Bian

Pacific Northwest National Laboratory, Richland, WA

Warren M. Washington

National Center for Atmospheric Research, Boulder, CO

Jongil Han and John O. Roads

Scripps Institution of Oceanography, La Jolla, CA

Corresponding author address: Dr. L. Ruby Leung, Pacific Northwest National Laboratory, P.O. Box 999, Richland, WA 99352; Phone: 509-372-6182; Fax: 509-372-6168; E-mail: ruby.leung@pnl.gov

Abstract. To study the impacts of climate change on water resources in the western U.S., global climate simulations were produced using the National Center for Atmospheric Research/Department of Energy (NCAR/DOE) Parallel Climate Model (PCM). The Penn State/NCAR Mesoscale Model (MM5) was used to downscale the PCM control (20 years) and three future (2040-2060) climate simulations to yield ensemble regional climate simulations at 40 km spatial resolution for the western U.S. This paper describes the regional simulations and focuses on the hydroclimate conditions in the Columbia River Basin (CRB) and Sacramento-San Joaquin River (SSJ) Basin. Results based on global and regional simulations show that by mid-century, the average regional warming of 1 to 2.5^{o}C strongly affects snowpack in the western U.S. Along coastal mountains, reduction in annual snowpack was about 70% as indicated by the regional simulations. Besides changes in mean temperature, precipitation, and snowpack, cold season extreme daily precipitation increased by 5 to 15 mm/day (15-20%) along the Cascades and the Sierra. The warming resulted in increased rainfall at the expense of reduced snowfall, and reduced snow accumulation (or earlier snowmelt) during the cold season. In the CRB, these changes were accompanied by more frequent rain-on-snow events. Overall, they induced higher likelihood of wintertime flooding and reduced runoff and soil moisture in the summer. Changes in surface water and energy budgets in the CRB and SSJ basin were affected mainly by changes in surface temperature, which were statistically significant at the 0.95 confidence level. Changes in precipitation, while spatially incoherent, were not statistically significant except for the drying trend during summer.

Because snow and runoff are highly sensitive to spatial distributions of temperature and precipitation, this study shows that (1) downscaling provides more

realistic estimates of hydrologic impacts in mountainous regions such as the western U.S., and (2) despite relatively small changes in temperature and precipitation, changes in snowpack and runoff can be much larger on monthly to seasonal time scales because the effects of temperature and precipitation are integrated over time and space through various surface hydrological and land-atmosphere feedback processes. Although the results reported in this study were derived from an ensemble of regional climate simulations driven by a global climate model that displays low climate sensitivity compared with most other models, climate change was found to significantly affect water resources in the western U.S. by the mid twenty-first century.

1. Introduction

The Accelerated Climate Prediction Initiative (ACPI) (DOE 1998) was funded by the U.S. Department of Energy (DOE) to develop the scientific knowledge and computational infrastructures needed to carry through an end-to-end assessment of the possible effects of human-induced climate change. A nested model approach in which effects of greenhouse warming are propagated through a suite of Global Climate Models (GCMs), Regional Climate Models (RCMs), and impact assessment models was used for an end-to-end assessment. To demonstrate the feasibility of this approach, water resources in the western U.S. were chosen as the primary focus of impact assessment of climate change.

There are important reasons to select the western U.S. and water resources for the demonstration. First, the population and economy of the western U.S. continue to grow fast. Planning for future resources is key to maintaining sustainable development of the region. Climate change is an important consideration in developing future plans because its impacts are potentially significant. Second, water resources are managed for multiple objectives such as flood control, hydropower production, irrigation supply, and fish protection that often conflict with one another. Historical climate variability has already been shown to significantly alter mean and extreme hydroclimate conditions of the Columbia River and Sacramento River (e.g., Gershunov and Barnett 1998; Mantua et al. 1997; Cayan et al. 1999). Climate change can significantly alter snowpack and streamflow in major river basins of the west (e.g., Leung and Wigmosta 1999; Hamlet and Lettenmaier 1999; Mote et al. 1999; Miller et al. 2002). Climate change will thus add

another constraint on the existing water management system. Information produced by an experimental end-to-end assessment can therefore be instrumental in establishing guidelines for management considerations and future studies. Third, the western U.S. is marked by complex terrain and diverse climate regimes. The value of downscaling in end-to-end assessment can be tested more suitably in relation to water resource applications in major river basins and watersheds of the region.

In the nested model approach used in end-to-end assessments, GCMs are used to produce simulations of current and future climate conditions. To bridge between spatial scales achievable by current GCMs (typically 150-300 km resolution) and those scales required by impact assessment, downscaling is used to produce climate projections at the regional scale. Studies have shown that the dynamically downscaled climate change signals retained the large-scale features of the global simulations. However, at the regional scales, the downscaled signals for temperature and precipitation can differ significantly from that produced by the GCMs, especially in regions with strong mesoscale forcings such as orography, lakes, and land surface heterogeneity (e.g, Whetton et al., 2001; Leung et al. 1999b; Giorgi et al., 1998; Laprise et al. 1998; Jones et al., 1997). In assessing the hydrologic impacts of climate change, differences between the climate change scenarios generated by GCMs and RCMs may lead to important differences in assessing water resources impacts.

Recent studies of climate change have begun to use the ensemble simulation technique to improve the signal-to-noise ratio for estimation of climate response (Cubasch et al. 2001). In the ensemble technique, small perturbations are introduced in the initial conditions to generate climate variability in an ensemble of climate

simulations. Each simulation is considered a possible realization of the future climate. Larger ensemble size reduces the confidence interval for the signal as noise is averaged out over more independent realizations. When downscaling is applied to the global climate simulations, however, ensemble technique has been rarely used because of computational constraints (see Giorgi et al. 2001 for a summary of recent regional climate change simulations).

A distinguishing feature of the ACPI pilot project is the use of ensemble simulations for both global and regional modeling as a measure of uncertainty in climate projections. That is, besides developing three ensemble global simulations of future climate, dynamical downscaling was performed based on a regional climate model (RCM) for each of the three ensemble global simulations. This paper presents regional climate change scenarios based mainly on the Penn State/NCAR Mesoscale Model (MM5) simulations. The MM5 model was evaluated in a hindcast mode by comparing long-term simulations driven by large-scale analyses against observations. Leung et al. (2002a&b) described various analyses and diagnostics of a 20-year simulation with MM5 driven by the NCEP/NCAR reanalyses. They focused on evaluating climate features for the western U.S. at 40 km spatial resolution. The MM5 produced realistic seasonal climate statistics such as mean and extreme precipitation over the region. The model also produced realistic mesoscale features of ENSO precipitation anomalies that resulted from interactions of large-scale circulation with the underlying topography. Section 2 describes the models and numerical experiments used to produce ensemble global and regional climate simulations. Section 3 provides a brief evaluation of the downscaled control simulation. Section 4 presents analyses of climate change signals for the western U.S. and

discusses uncertainty in the climate signals based on ensemble simulations with the MM5 and comparison with a set of simulations by another regional climate model. Our analyses were focused mainly on aspects of the simulations that were important for hydrologic consideration, which is the theme of the ACPI end-to-end assessment. Section 5 summarizes the findings and implications and discusses potential research paths for future studies.

It should also be noted that the downscaled results were used to drive various process models to study mid-century effects of climate change on water resources in the western U.S. These are described in a number of other papers in this same issue. Interested readers may refer to these papers for a comparison of hydrologic impacts derived directly from the regional climate model (this paper) and those derived from hydrologic models driven by the global and/or regional climate simulations reported in this paper. Hydrologic simulations were performed at spatial resolutions typically 5 to 10 times higher than that of the regional models and bias correction was applied to the climate scenarios to ensure more realistic simulations of runoff under the control climate.

2. Numerical Experiments

The models and numerical experiments used to simulate global and regional climates are described in subsections 2.1 and 2.2.

2.1. GLOBAL CLIMATE SIMULATIONS

The global climate model used to simulate the control and future climate conditions was the National Center for Atmospheric Research/Department of Energy Parallel Climate

Model (NCAR/DOE PCM) described in Washington et al. (2000) and Dai et al. (2002). The model was developed jointly by Los Alamos National Laboratory (LANL), the Naval Postgraduate School (NPG), the US Army Corps of Engineers' Cold Regions Research and Engineering Lab (CRREL) and the National Center for Atmospheric Research (NCAR). It consists of the NCAR Community Climate Model version 3 (CCM3), the LANL Parallel Ocean Program (POP), and a sea ice model from the Naval Postgraduate School coupled together in a massively parallel computer environment. The atmospheric component, the NCAR CCM3, includes its latest versions of radiation, boundary layer physics, and precipitation physics. CCM3 also includes a comprehensive land surface model (LSM), which takes into account soil physics and vegetation.

The moderate resolution global ocean model uses the POP model with a displaced polar grid. The grid has an average resolution of 2/3 degree and increased latitudinal resolution near the equator of approximately 1/2 degree. Because of the displaced pole, there is relatively higher horizontal resolution in the eastern North Pacific, the Arctic Straits near northern Canada and Greenland, and the Gulf Stream area. The continents and bottom topography were carefully modified to obtain realistic flow in many regions throughout the globe. The model in its present form yields a reasonable simulation of the Arctic Ocean, tropical Pacific, and various boundary currents, such as the Gulf Stream, with some eddy-like activity in most basins. The elastic viscous plastic sea ice model uses a grid spacing of 27 km to represent small-scale features such as ice transport through the Canadian Archipelago and the East Greenland current region.

The three component models are tied together through a flux coupler, which performs interpolations between the different grids of the component models, handles

data transfer between component models, and ensures conservation of the various interfacial fluxes. Flux adjustments are not used in the PCM.

Washington et al. (2000) reported experiment results from a 300-year present-day coupled climate control simulation and transient 1% per year compound CO_2 increase. In particular, a global warming of 1.27 °C occurred for doubled CO_2 and 2.89°C occurred for quadrupled CO_2. Barnett et al. (2001) reported that the PCM was able to reproduce both the observed change in global air surface temperature and ocean heat content because of its relatively low climate sensitivity. They argued that models with higher climate sensitivity might have difficulty satisfying the ocean constraint. The results reported in this study should therefore reflect the impacts of climate change based on projections by a model with low climate sensitivity.

In the ACPI pilot study, PCM was used to simulate the control and future global climate conditions at T42 spatial resolution. These simulations were initialized using assimilated ocean conditions for 1995 (Pierce et al. 2002). In the control simulation, which lasts for 80 years, concentration of CO_2 (358 ppmv) and sulfate aerosols were kept constant at the 1995 level throughout the simulation. Three ensemble simulations of future climate conditions were then performed, except the concentrations of CO_2, other greenhouse gases, and sulfate aerosols follow that of the IPCC business-as-usual (BAU) scenario between 1995-2100 (Dai et al. 2001a&b). Each simulation of the ensemble was initialized using different atmospheric conditions to generate three possible realizations of the future climate. Climate change signals were estimated based on differences between the ensemble mean of the future climate conditions and the control simulation. Since warming continues during the 80 years in the control simulation as the climate

system is transitioning to a state that is in equilibrium with the 1995 CO_2 and sulfate aerosols forcings, there was a warming of up to 1°C in the western U.S. comparing the mean of the control simulation with the 1995 condition.

PCM simulation data were archived at three temporal frequencies. Two- and three-dimension instantaneous data needed for driving dynamical downscaling models were archived at 6-hourly intervals. Variables related to the surface energy and water budgets and outputs of the land surface models were archived as 6-hourly and daily averages. A long list of output variables was also archived as monthly averages.

2.2. REGIONAL CLIMATE SIMULATIONS

To obtain regional climate conditions for climate impact assessments, dynamical downscaling was performed using the MM5 (Grell et al. 1993). Leung et al (2002a&b) described in detail the model configuration and simulation results when the MM5 was driven by NCEP/NCAR reanalyses for 20 years. The same model configuration was also used in this climate change study. The nested configuration consists of a large domain that covers the U.S., part of Canada and Mexico, and the surrounding ocean at 120 km resolution and a nested domain at 40 km resolution that was used to produce higher resolution simulation for the western U.S. Figure 1 shows the grid cell locations of the PCM and MM5 within the nested domain. Also outlined in the figure are the boundaries of the Columbia River Basin (CRB) and Sacramento-San Joaquin (SSJ) River Basin, which are the study regions of the ACPI impact assessment. There are roughly 14 and 4 PCM grid cells and 386 and 104 MM5 grid cells within the CRB and SSJ basin

respectively. At 40 km spatial resolution, the terrain features of the western U.S. are realistically represented and the basins are well resolved by many grid cells.

The MM5 preprocessor was modified to convert PCM outputs to create initial and boundary conditions for running MM5. The lower and lateral boundary conditions were updated every 6 hours based on large-scale conditions of the global simulations. Large-scale variables used in the boundary conditions include temperature, wind, water vapor mixing ratio, geopotential height, sea level pressure, and sea surface temperature from the PCM simulations. Physical processes represented in the MM5 include cumulus and shallow convection, mixed-phase cloud microphysics, longwave and shortwave radiation, turbulence transport, and land surface physics. Leung et al. (2002a) described the choices of physics parameterizations used in the simulations. In particular, differences between the OSU Land Surface Scheme used in MM5 and the Land Surface Model (LSM) used in PCM may account for some differences between surface variables in the global and regional simulations.

The MM5 was used to downscale the control simulation that was initialized in 1995 for the first 20 years and each of the three ensemble future climate conditions for 2040-2060 to elucidate mid-century effects of greenhouse warming. The ensemble simulations differ from one another because of differences in initial and boundary conditions provided by the PCM. According to the BAU scenario, the concentration of CO_2 in the atmosphere increases from 358 ppmv in 1995 to 505 ppmv in 2050. Because changes in temperature and precipitation during the first 20 years of the control run was negligible, we have assumed that the control simulation is representative of the climate conditions of the 1990s. All global and regional climate simulations were performed on

an IBM-SP3 at the Oak Ridge National Laboratory using 64 processors. Different variables were archived at 3-hourly, 6-hourly, and daily intervals for climate analyses as well as for providing inputs to impact assessments.

Besides using ensemble simulation technique to estimate uncertainty in the climate projections, we also compared the MM5 downscaled simulations with regional simulations produced by the NCEP Regional Spectral Model (RSM) (Juang and Kanamitsu 1994; Hong and Leetmaa 1999; Roads and Chen 2000; Roads et al. 2002). The RSM domain covers the whole U.S. with an average resolution of 50 km. Leung et al. (2002c) provide more details about the configuration of the RSM model and describe a comparison of MM5 and RSM simulations driven by global reanalyses for the western U.S.

Two PCM simulations were used to drive the RSM to yield regional climate change scenarios. The first PCM simulation was based on a historical run initialized in 1870 using historical CO_2 concentrations. Downscaling was performed for 10 years between 1986-1996. The second PCM simulation was a continuation of the historical run projected into the future (2100) using CO_2 and aerosol concentrations of the BAU scenario. These PCM scenarios differ from those used in the MM5 downscaling in that ocean conditions were simulated by the PCM in the historical run rather than assimilated for initializing the PCM in the control and future climate scenarios. The latter set of PCM simulations were not available at the time RSM downscaling was performed. The RSM downscaling of future climate was performed for 10 years between 2040-2050. RSM outputs were archived every 6 hours and compared with the MM5 simulations. Table 1

summarizes the models and characteristics of the global and regional simulations discussed in this paper.

3. Control Simulations

The control simulation used to drive the MM5 corresponds to climate conditions that are in transition to equilibrium with the CO_2 and sulfate aerosol forcings of 1995. As such, the simulation cannot be compared directly with historical climate conditions. Nevertheless we find that, for the western U.S., the first 20 years of the control simulation do not differ greatly from the PCM historical simulation of 1975-1995. This is illustrated in Figure 2, which shows the annual mean temperature and precipitation averaged over the CRB and SSJ basin for the control and historical simulations. The mean annual temperature and precipitation of the control simulation (1995-2015) are well within 0.3^{o}C and 15% of the historical simulation (1975-1995) in many areas within the CRB and SSJ basin. In what follows, we will compare the PCM and MM5 control simulations directly with observations of the past 20 years as an indication of model performance.

Figures 3 and 4 show the spatial distributions of seasonal mean temperature and precipitation as observed and simulated by PCM and MM5. Observations were based on a 1/8° gridded dataset for 1980-2000 derived from station data using the method described by Maurer et al. (2001). Spatial interpolation was performed based on the statistical topography-precipitation relationships developed by Daly et al. (1994) to account for orographic precipitation in the western U.S. The PCM simulation was

bilinearly interpolated from the PCM grid to the MM5 nested grid for this comparison. During winter, the PCM simulated precipitation shows a gradual reduction in precipitation from the Pacific coast inland. The RCM simulation depicts a much more realistic spatial distribution of cold season precipitation than the PCM simulation in the western U.S. The simulation clearly distinguishes the regional maxima related to coastal mountains (e.g., the Olympic Mountain) and the Cascades and Sierra Ranges. Similar to the observations, secondary peaks are also found over the Northern Rockies, the Wasatch Range, and the Colorado Plateau. The RCM precipitation was generally more widespread than the observations. The regional control simulation is surprisingly similar to the regional simulation driven by 20 years of NCEP/NCAR reanalyses shown in Figure 2 of Leung et al. (2002a).

During the warm season, the PCM simulation shows a strong precipitation maximum over the central Rockies that extends northward across the U.S.-Canada border. In the regional simulation, the precipitation maximum was totally removed and the spatial distribution became more realistic compared to the observed pattern. The large differences between the PCM and RCM simulated precipitation during summer were related in part to the different convection schemes used in the models. Negative biases occurred along northwest mountains and in the southwest monsoon region. For surface temperature, both the PCM and RCM simulations reproduced the observed temperature rather well, with the latter capturing more realistically the spatial distribution affected by topographic features. Biases between the simulated and observed temperature were generally within 3°C.

Figure 5 shows the mean annual cycle of temperature and precipitation from observations and the PCM and RCM control simulation averaged over CRB and SSJ. In CRB, the simulated seasonal cycles of temperature were very close to the observed except during spring (February – May) where cold biases of up to 5°C occurred. In SSJ, there were cold biases during winter and warm biases during summer that were within 4°C. At the larger scales such as the entire CRB and SSJ basin, the downscaled simulation was within 2°C of the PCM simulation. For precipitation, the seasonal cycle was well represented in CRB by the PCM and RCM simulations. However, in SSJ, the RCM produced much more precipitation between January and March than the PCM simulation and the observation. The cold season wet biases were generally less than 50%.

4. Climate Change Signals

The following analyses were based on results from the global (PCM) and regional (MM5) climate simulations. Climate change signals were calculated as the differences between ensemble means of the three future climate simulations between 2040-2060 and the 20-year control simulation. This paper focuses on changes in the hydrologic cycle that affect water resources in the western U.S.

4.1. TEMPERATURE

Figure 6 shows the seasonal mean signals in surface air temperature over the western U.S. as simulated by PCM and MM5. Surface air temperature from MM5 was calculated based on a simple weighting of surface skin temperature and air temperature at the

model's lowest level (near 40 m) following Dickinson et al. (1986). In PCM, surface air temperature was estimated at the reference height of 2 meters over land and 10 meters over ocean. During summer the warming was between 1.5 - 2°C and stronger inland. In the RCM during winter, the warming was stronger along coastal mountains such as the Cascades and the Sierra, and on the northern latitudes. This warming is consistent with reduced snow-albedo feedback effects along the coastal mountains because less snow is accumulated under the greenhouse warming scenario. In the PCM, stronger warming is found over the Rockies in the winter, which is also consistent with reduced snow-albedo effects because the PCM only resolved topographic features and snow in the Rockies and not the narrow coastal ranges. Because the RCM simulated snow cover was much more realistic than the PCM, the spatial pattern of temperature change simulated by the RCM could arguably be more realistic. Similar spatial patterns of temperature change were also found for spring (not shown) when snow effects were apparent. The temperature signals were statistically significant at the 0.95 confidence level based on a two-tailed t-test for all seasons and regions. Temperature change was generally less in the downscaled scenarios than the PCM scenarios.

To further investigate the change in temperature, Figure 7 shows the frequency distribution of daily mean surface temperature for six regions shown in Figure 1 based on the control and future RCM simulations. During winter, there was a clear asymmetry in the frequency distributions, especially in regions 1 to 4, showing negative skewness with long tails at the lower ends. In the future climate, the negative skewness increased such that warming on the higher ends or warm days was less than warming on the lower ends or cold days. The change in the 95th percentile daily mean temperature was found to be 1

to 2°C lower than that in the 5th percentile in most places. The frequency distributions of daily mean temperature during summer were typically narrower and had shorter tails than winter. Similar to changes found in winter, there was also a tendency for increased negative skewness in the future climate. Greenhouse warming therefore brings milder conditions in the western U.S. to extreme low temperature and only moderately increases extreme high temperature.

Figure 8 shows the diurnal temperature range (DTR) for the six regions based on the RCM simulations. During winter, the simulations showed a positive skewness in DTR in the Northwest (regions 1, 2, and 3). In those areas, there was a higher frequency of small DTR corresponding to frequent cloudy days. This tendency and the physical constraint for DTR to be above zero led to the positively skewed distribution. Large DTR values between 20 to 25°C were more likely a result of frontal passage causing significant temperature drop than radiation effect which was limited during winter at the higher latitudes. There was a small tendency of increased positive skewness or a shift in the peak towards lower DTR in the future. In regions 4, 5, and 6, DTR had a much broader, more symmetrical and near bimodal distribution. The bimodal feature could be related to bimodal distribution of cloudiness that depended on the location of the jet stream and frequency of frontal passage. Clearly the Southwest was marked by higher frequency of larger DTR that corresponded to clear days than other regions. Under climate change, there was a reduction in the frequency of the first peak at the lower DTR range and an increase in the frequency of the second peak at the higher DTR range, suggesting increased frequency of clear days. The latter was consistent with reduced precipitation in those regions.

During summer, the distribution of DTR in the Northwest (regions 1, 2, and 3) became less positively skewed and more Gaussian like. There was a shift towards slightly larger DTR in the future than the control. The distributions of DTR in regions 4, 5, and 6 went through a large transition from winter to summer. Instead of the broader or bimodal distribution found during winter, the summer DTR distribution was negatively skewed and more concentrated over a certain range. The negative skewness was related to the upper physical constraint determined by clear sky radiation heating or cooling. Similar to the Northwest, there was a tendency of shift towards larger DTR in the future climate, suggesting increased frequency of clear days.

4.2. MEAN AND EXTREME PRECIPITATION

Figure 9 shows the ensemble mean changes in seasonal mean precipitation based on the PCM and RCM simulations. During the cold season, precipitation in the western U.S. was mainly driven by large-scale circulation bringing in abundant moisture from the Pacific Ocean. In the downscaling procedure, the RCM correctly preserved the PCM large-scale features, showing wetter conditions in the northeastern side of the domain and drying trend near the Pacific coast that were comparable to the characteristics of the PCM signal. Differences between the PCM and RCM spatial patterns at the regional scale such as the much stronger drying trend along coastal mountains were caused by mesoscale forcings such as topography. Leung et al. (2002b) showed that because of its ability to resolve the interactions between large-scale circulation and orography, the RCM captured realistic mesoscale precipitation anomaly patterns related to large-scale circulation anomaly during the warm phase of the El Nino-Southern Oscillation. One may therefore

argue that the RCM also produced more realistic cold season regional precipitation changes that were consistent with the large-scale circulation change produced by the PCM under climate change. During the warm season, precipitation was less dependent on large-scale circulation and differences between the spatial distributions of the PCM and RCM precipitation signals were more likely related to differences between the physics parameterizations used in the models than regional forcings.

Based on Figure 9, precipitation changes were generally less than 1 mm/day for all seasons. Larger changes were found during the cold season in northern California and along the coast of British Columbia. The drying in California projected by the PCM and RCM in this study should be contrasted with the wet trend based on the Hadley Centre Model and Canadian Model reported in the National Assessment Report (2000). However, because of strong variability, most changes shown here were not statistically significant at the 0.9 confidence level based on a two-tailed t-test performed for each grid cell except for the drying trend during summer, the wetter conditions over the Northern Rockies during fall and winter, and the drying trend in the Great Basin during spring (not shown). Strong variability in precipitation was reflected in large differences in the spatial distribution of precipitation signals among ensemble members and between each 10-year period (2040-2050 versus 2050-2060) (not shown). That is, depending on which ensemble simulation and which 10-year period was analyzed, the simulated precipitation changes were highly variable spatially. We conclude that results based on shorter simulations or a single simulation are somewhat misleading in defining the precipitation signal under greenhouse warming in the western U.S.

Changes in the 95th percentile extreme daily precipitation based on MM5 simulations are shown in Figure 10 for the summer and winter seasons. Extreme precipitation was calculated based on simulated daily precipitation excluding no rain days with precipitation amount less than 0.01 mm/day. During winter, extreme daily precipitation increased by up to 10 mm/day at the Cascades and Sierra. This corresponds to 15-25% increase in those areas. There were also increases between 15-30% extensively over the Northern Rockies. Combined with existing snow conditions in these mountainous areas, enhanced extreme precipitation can increase the severity of wintertime flooding corresponding to rain on snow events. During summer, extreme precipitation was reduced along the Sierra, southern California, and coastal region of Oregon by 3-20 mm/day, which corresponds to reductions of 25-35%. Extreme precipitation was increased in the British Columbia by 10-25%. During both seasons, there was a small increase in the number of no rain days (using a threshold of 0.01 mm/day) over most of the western U.S. by mid-century.

4.3. SNOWPACK AND RUNOFF

A robust feature of the climate change signal in the western U.S. was the reduction in mountain snowpack caused mainly by warmer temperatures projected for the future. Figure 11 shows the absolute and percentage changes in annual snowpack in the western U.S. simulated by PCM and MM5. Annually significant reductions in snowpack were found along the Cascades, the Sierra, and the Northern Rockies by 10-100 mm. Percentage changes were largest along the coastal ranges where snowpack was reduced by 60-70% compared with 20% reduction in the Northern Rockies. The spatial

distribution of snowpack changes was more realistically simulated in mountain regions by MM5 than PCM, mainly because PCM did not resolve coastal mountains and consequently, it could not produce realistic precipitation and snowpack associated with the orography.

As discussed by Leung and Ghan (1999b), the big contrast in snowpack reduction along coastal mountains versus inland mountains was due to differences in cold season temperature between the maritime and continental climate. Warming of 1-2°C can reduce snowpack significantly along the Cascades and Sierra where winter temperatures are typically close to freezing. In the Northern Rockies, the same warming will probably have a much smaller effect because winter temperatures are normally much below freezing. Because of snow-albedo feedback effects, the larger reduction in snowpack along coastal mountains was reflected in stronger warming during the cold season than that over inland mountain (see Figure 6). During March (not shown) large reductions of 70% were found over most of the western U.S. except for the central and Northern Rockies.

In the western U.S., impacts of climate change on water resources depend not only on separate mean changes in temperature and precipitation. The change in the joint distribution of temperature and precipitation is also of hydrological significance. For example, increase in precipitation in regions with larger warming (such as along coastal mountains because of snow-albedo feedback) will have effects different from precipitation increase in regions with moderate warming because temperature affects the phase of precipitation and snow accumulation at the surface. In Table 2, we show the basin-mean changes of other variables as a result of changes in temperature and

precipitation. There are large changes in mean and extreme precipitation and runoff, precipitation frequency and intensity, snowfall, and rain-on-snow events; the latter is a main cause of winter floods in the Northwest and northern California. A threshold of 0.01 mm/day was used to define rain days for calculating precipitation frequency and intensity. Snowfall and rain-on-snow events were determined using 3-hourly surface temperature and precipitation data where a threshold of $0^{o}C$ is used to distinguish rainfall from snowfall. Rain-on-snow events occurred when rainfall (> 0.01 mm/day) happened with existing snowpack. Rain-on-snow amount was calculated as the averaged amount of rainfall during rain-on-snow events, and the frequency of rain-on-snow events was calculated as the number of rain-on-snow events over the total number of three-hour periods used in the estimation.

Table 2 shows that percentage changes in seasonal mean precipitation were very small except for June-July-August (JJA) where precipitation was reduced by more than 20%. Although mean precipitation and precipitation frequency were typically reduced during the cold season, the 95th percentile extreme daily precipitation and mean precipitation intensity were generally increased. This suggests a shift in the probability distribution towards more intense precipitation during winter under future climate. Furthermore, although changes in precipitation were small, the warming signal significantly lowered the proportion of snowfall in the total precipitation in the CRB (reduced by 20%) and SSJ basin (reduced by 30%) to reduce snow accumulation. In the control climate, about 50-70% and 20% of precipitation were snowfall respectively in the CRB and SSJ basin between December and May.

In terms of runoff, there was an increase of 40% during December-January-February (DJF) and reduction of 28% during March-April-May (MAM) in the CRB. The increase in the proportion of rainfall over snowfall and rain-on-snow events were responsible for the larger runoff during winter. In the control simulation, about 12% of precipitation fell during rain-on-snow events in the CRB. With an increase in the frequency of rain-on-snow events by about 10% throughout the winter in the CRB, more rapid snowmelt can result. This was reflected in 11% increase in the 95th percentile extreme runoff shown in Table 2.

In the SSJ basin, the reduction in snowfall is even more severe. There was a reduction of more than 30% throughout the cold season because of warmer temperatures. In the control simulation, only about 4% of precipitation fell during rain-on-snow events. Unlike the CRB, the frequency of rain-on-snow in the future climate was reduced because the probability of finding snowpack on the ground was greatly reduced. Still, runoff was enhanced during the winter because increasing rainfall over snowfall contributed directly to runoff. During spring, runoff was reduced by 7% because of reduced snowmelt. The 95th percentile extreme daily runoff was increased by 43% in September-October-November (SON) and 14% in DJF. While climate change impacts on cold season floods were stronger during DJF in the CRB, more significant impacts were found during SON in the SSJ basin. In both basins, climate change had negative impacts on water supply during spring and summer.

4.4. SURFACE ENERGY AND WATER BUDGETS

Accompanied by changes in temperature and precipitation are changes in all components of the surface energy and water budgets. To illustrate changes in the seasonal cycle of the energy and water partition, we calculated the CRB and SSJ basin mean monthly changes of precipitation, total runoff, evapotranspiration, and soil moisture and snowpack accumulation for the surface water budget. For the surface energy budget, we calculated the sensible and latent heat flux and net shortwave and longwave radiation at the surface. Figure 12 shows the changes in the components of the surface water budget under greenhouse warming by mid-century.

In the CRB, precipitation changes were small throughout the seasonal cycle. This suggests that changes in other components of the water budget were mostly driven by changes in temperature rather than precipitation. As a result of warming, there were significant reductions in snowpack between December and May, which were reflected in reduced snow accumulation between November and February and less snow melt between March and May in Figure 12. Note that snow accumulation rate (SP) is denoted positive and snowmelt is negative. In snow-dominated basin such as CRB, changes in runoff reflect the changes in both precipitation and snow accumulation or melt. Therefore, while changes in runoff and precipitation should be similar on an annual basis, they can differ on a monthly basis. As shown in Figure 12, runoff increases during January and March occurred because in the warmer climate more precipitation came in the form of rain rather than snow. By contributing directly to runoff or by causing snowmelt, a higher percentage of rainfall versus snowfall during the cold season increased runoff. As less snow was accumulated during winter, runoff as a result of snowmelt between April and June was reduced. Changes in runoff were also reflected in

a shift in peak runoff from May to April in the future climate scenarios as a result of earlier snowmelt. Changes in soil moisture followed a pattern similar to the runoff. During winter, increased rainfall and runoff enhanced soil moisture. Between May and November, soil moisture accumulation was reduced because of reduced snowmelt and increased evapotranspiration caused by warmer temperatures.

In the SSJ basin, precipitation changes were larger during the cold season than that in the CRB. However the signs of the changes were not consistent throughout winter. Because of warmer temperature in the future scenarios, snowpack was also reduced in the SSJ basin although it was not as significant as in the CRB. Runoff changes responded more directly to changes in precipitation in a warmer climate regime. Nevertheless the effects of warming on the rain versus snow were also reflected in increased runoff between December and January even though precipitation changes were negative. There was also a shift in peak runoff from March in the control simulation to February in the future climate conditions as a result of earlier snowmelt. Soil moisture was basically reduced throughout the year except in November. These reductions were caused by a warmer climate, which also could enhance evapotranspiration despite larger runoff during January and February.

Figure 13 shows the changes in surface energy budget in the two river basins. In both basins, net shortwave radiation at the surface was mainly balanced by sensible heat flux and net longwave radiation during summer and latent heat flux and net longwave radiation during winter. Under the future climate scenarios, changes in each component of the surface energy budget were rather small. During winter, net shortwave radiation increased perhaps as reduced snow accumulation lowered the surface albedo. Sensible

heat flux, latent heat flux and net longwave radiation all decreased by 1 – 3 W/m^2. During summer, sensible heat flux increased by 4 – 8 W/m^2 in response to the warmer temperature. Changes in other surface energy components were less clear because their magnitudes were small and changes in sign were often different during the year.

Table 3 summarizes the changes in surface energy and water budgets in the PCM and MM5 climate change simulations averaged over the CRB and SSJ basin. A comparison of the changes at the larger scale of the PCM and the regional scale of the MM5 revealed the importance of downscaling in simulating impacts on water resources in the western U.S. Although differences between the basin-mean temperature and precipitation changes simulated by PCM and MM5 were relatively small, much larger differences were found in snowpack and runoff simulated by the two models. The PCM simulated changes in snowpack were much smaller than that of the MM5, and the difference is larger in SSJ than CRB.

Differences between the PCM and MM5 results occurred because of differences in land surface parameterizations used in the global and regional models and differences in spatial resolutions. The impacts of the former are more difficult to assess. For the latter, at higher spatial resolution, MM5 was able to simulate more realistically the spatial distributions of temperature and precipitation that were strongly affected by the complex topography of the western U.S. Other energy and water components such as snow and runoff were redistributed spatially in response to changes in these quantities. Because of nonlinear processes in land surface energy and water exchange, even basin-mean changes in surface energy and water budgets can become significantly different for models

applied at different spatial resolutions. Downscaling therefore ensures more realistic climate sensitivity to be simulated for the surface water and energy budgets.

4.5. UNCERTAINTY BASED ON ENSEMBLE SIMULATIONS

Because of computational constraints, most climate change studies in the past have relied on single realizations. In this study, three ensemble simulations were performed using both the global and regional models to obtain projections of future climate. Figure 14 shows the annual mean temperature and precipitation based on the three PCM climate change simulations in the CRB and SSJ basin for 1995-2100. There was large interannual variability simulated by the model for the western U.S. For surface temperature, the standard deviation of the annual mean temperature was about 1-1.5^{o}C and was larger in the CRB than SSJ basin. All three simulations followed a similar linear trend in temperature rise as CO_2 increases throughout the simulation period. For precipitation, the ratio of the standard deviation to the mean of the annual mean was larger in the SSJ basin (60%) than the CRB (25%). A similar variation occurred for temperature and precipitation variability in the CRB and SSJ basin in historical records (i.e., temperature variability is larger in the CRB but precipitation variability is larger in the SSJ basin; see e.g. Leung et al. 2002b). There was almost no linear trend in precipitation, although interannual variability did appear to increase during the mid-century in the SSJ basin.

Based on Figure 14, it appeared that differences among ensemble simulations were small compared to the strong interannual variability simulated by the model. Figure 15 shows the temperature and precipitation signals averaged over the CRB and SSJ basin based on each member of the ensemble regional simulation. Each curve represents the

mean signal calculated based on the difference between the mean monthly temperature or precipitation averaged over 20 years of each future (2040-2060) and the control simulation. The standard deviation of each mean signal was calculated based on the square root of the sum of variance of the mean monthly temperature or precipitation for each future simulation and the control simulation. It represents the standard deviation of the mean climate signal for each pair of ensemble control and future simulations.

Differences among mean monthly warming signals based on each ensemble simulation were 0.25–1.0^{o}C, which were about 10-40% of the ensemble mean. Generally each mean monthly signal fell within the standard deviation of the mean monthly signal based on other members of the ensemble simulation for the same month. This suggests that variability among ensemble members were within the variability captured by 20 years of a single simulation. Precipitation differences were between 0-0.5 mm/day in the CRB and 0-1.5 mm/day in the SSJ basin, which were between 0-200% of the ensemble means. Again these differences were generally within the standard deviations of each ensemble run. Exceptions occurred during winter and spring (e.g., January and March through May in the CRB and March and April in the SSJ basin) where ensemble differences exceeded the standard deviations. Larger ensemble sizes will be needed to better characterize uncertainty in the precipitation signals.

Figure 16 shows the signal-to-noise ratio of the cold season mean temperature and precipitation based on the PCM and RCM simulations. The RCM signal-to-noise was consistent with that of PCM at the larger scale. Although the RCM simulations showed more structures in climate signals such as the stronger warming and precipitation changes along the Cascades and Sierra at the regional scale, the magnitude of the signal-to-noise

ratio was not significantly different from that of PCM. This is because climate variability was large along the Cascades and Sierra where the signals were large. This suggests that in this region of complex terrain, regional forcings amplified both climate change signals and climate variability. As a result, predictability of climate change signals was neither improved nor degraded by the orography.

4.6. UNCERTAINTY BASED ON TWO SETS OF DOWNSCALING EXPERIMENT

To extend the characterization of uncertainty in climate projections, the ACPI pilot project included the NCEP Regional Spectral Model (RSM) for downscaling of the PCM climate change simulations. However, the RSM simulations were performed using a different set of PCM simulations, as described in 2.2 and Table 1. Therefore a detailed comparison of the RSM and MM5 climate change signals is difficult because: (1) they are not based on the same PCM simulations; (2) they are not of the same length and ensemble size; and (3) there are differences between RSM and MM5 in terms of dynamical and physical representations, model domain, and spatial resolution (Leung et al. 2002c). Nevertheless, a comparison of the MM5 and RSM scenarios for the same region and time period can provide a broader perspective on uncertainty of climate projections for the western U.S.

Before we investigate the differences between the MM5 and RSM climate change signals, it is useful to summarize what differences might be expected from results based on these models. Leung et al. (2002c) noted a large difference in the spatial distribution of cold season precipitation between MM5 and RSM simulations driven by global reanalyses. Because RSM uses a spectral representation, topography is more strongly

smoothed compared with MM5 even at similar spatial resolutions. Topographic features such as the Cascades and Sierra were not well resolved by RSM. As a result, MM5 produced stronger orographic precipitation in the Cascades, the Sierra, and northern Rockies, and RSM generated more precipitation along the low-lying coastal area instead. During summer, RSM produced more precipitation in the northern Rockies than MM5. These differences in precipitation simulations were found to be associated more with differences in physics parameterizations, model formulations, and topographic representations between RSM and MM5 than the driving large-scale conditions.

Figure 17 shows the temperature and precipitation signals simulated by RSM based on the difference between 2040-2050 and 1986-1996. A comparison of Figure 17 with the climate change signals simulated by MM5 (Figures 6 & 8) shows some interesting differences in spatial characteristics between the RSM and MM5 climate signals. For temperature, the MM5 signals showed stronger warming along the Cascades and the Sierra during winter due to snow-albedo feedback effects. Such enhanced warming was not found in the RSM simulations. For precipitation, the MM5 winter signals again displayed more spatial structures related to topography of the coastal mountains than the RSM signals. During summer, changes in the RSM were generally larger, especially over the northern Rockies. Note that these differences were not related to the difference in time periods (2040-2050 in the RSM versus 2040-2060 in the MM5) or ensemble sizes (one in RSM versus three in MM5) because similar differences were found comparing each MM5 ensemble simulation with the RSM simulation for the same period. They are mainly related to differences in topography and physical parameterizations used in the models, which affect the simulations of orographic and

convective precipitation and their interactions with other processes. Both RSM and MM5 showed little areas with precipitation signals at or higher than 95% confidence level during winter. During summer, both showed more extensive areas with significant increase in precipitation, although the RSM signals were generally much larger. For temperature, the lack of statistical significance in the RSM signals is partly related to the shorter simulation period and weaker warming during winter.

Figure 18 shows the CRB and SSJ basin mean climate change signals in surface temperature and precipitation based on the RSM and MM5 simulations. Climate change signals for the RSM simulations were calculated simply by differencing the monthly temperature or precipitation averaged over 10 years of the future and control simulations. The climate change signals are all shown for the same period in the future (2040-2050). Results from PCM are shown in black and those of MM5 and RSM are shown in grey using the same line pattern for each pair of PCM and regional simulation.

Based on the simulated temperature signals, several general observations can be made. First, during the warm season, the downscaled monthly signals were typically smaller than that of the PCM by up to 1°C. Second, averaging over the annual cycle, the difference between the PCM and downscaled temperature signals was very small for the PCM-MM5 experiments; for the PCM-RSM experiment, the downscaled signal was up to 0.53^{o}C or 43% colder than the PCM signal. Third, because the mean monthly signals were calculated based on only 10 years rather than 20 years, differences among ensemble members were larger than those in Figure 14. Fourth, because of strong interannual variability and low PCM climate sensitivity, mean monthly signals were sometime negative (cooling) or near zero if only 10 years of an earlier period (2040-2050 rather

than 2050-2060) were used in the estimation. Lastly the PCM-RSM experiment exhibited the mildest warming of all experiments.

Changes in mean monthly precipitation were usually very small. Figure 18 shows that differences among simulations were especially large during November to January in the CRB and December to February in the SSJ basin. The precipitation signals could be positive or negative depending on which pair of PCM and downscaling experiment was used. These levels of uncertainty could be overcome by extending the time period or increasing the number of simulations. Similar to temperature signals, the difference between PCM and downscaled precipitation signals were usually larger for the PCM-RSM pair than the PCM-MM5 pairs. However, all regional models amplify the precipitation signals from the PCM as a result of strong topographic forcings within the basins.

Further differences among the four downscaling experiments are seen in the spatial distribution of changes in March snowpack simulated by each MM5 and RSM experiment for 2040-2050 (not shown). Because snowpack is highly sensitive to temperature and precipitation, small differences among the ensemble MM5 and RSM projections can result in large differences in projecting snowpack changes. Along the Cascades and the Sierra, reductions in March snowpack were most significant (over 100 mm or 80%) for MM5 simulations 1 and 2, where temperature changes during the cold season were stronger than other simulations. The spatial distributions of the change were similar among the MM5 simulations. In the RSM simulation, reductions in snowpack were not only smaller, they were distributed mainly in the Northern Rockies rather than along coastal mountains. Because RSM produced less orographic precipitation than MM5

as discussed above, it simulated two to ten times less snowpack than MM5 on the Cascades and the Sierra. Therefore, depending on the climate projections based on different sets of models and numerical experiments, climate change effects on water resources in the western U.S. can vary strongly in terms of magnitude and spatial distribution, despite general agreements in the directions of the trends.

5. Conclusions

This paper described dynamical downscaling of ensemble global simulations of present and future climate conditions. Because of the complex topography and diverse climate regimes, downscaling was shown to be important for realistically capturing regional climate in the western U.S. (e.g., Leung et al. 2002a). Comparing the PCM and MM5 control simulations, spatial distributions of precipitation, temperature, and snowpack were much more realistically simulated at the higher spatial resolutions in the regional models. Downscaling did not significantly alter regional mean changes in temperature and precipitation. Nevertheless differences between the spatial distributions of temperature and precipitation signals in the global and regional simulations were sufficient to induce large differences between the PCM and MM5 basin-mean surface energy and water budgets in mountainous basins.

At higher spatial resolution, changes in snowpack and runoff were much larger in the regional simulations than the PCM simulations where coastal mountains such as the Cascades and the Sierra were not resolved. We found that snow-albedo feedback effect could cause a stronger regional warming over coastal mountains. Such elevation

dependence in temperature signals has been described in previous regional studies of climate change effects (e.g., Giorgi et al. 1997; Leung and Ghan 1999b; Kim 2001).

There were a few significant changes that seem to be robust among the ensemble simulations. First, as a result of warming by mid-century, which was statistically significant at the 0.95 confidence level over most of the western U.S., more precipitation fell in the form of rain than snow (10 to 20% reduction in snowfall in the CRB and over 30% reduction in the SSJ basin). This reduction in snowfall together with increased snowmelt due to warmer temperature acted to reduce snowpack accumulation during winter in the basins. At the same time, an increased proportion of rainfall over snowfall and increased snowmelt due to warmer temperatures contributed directly to increased runoff. In the CRB, this was exacerbated by an increase of over 10% in rain-on-snow events that caused rapid snowmelt. During spring and early summer, runoff was reduced because of reduced snowpack in the mountain. Changes in runoff were therefore manifested in a large seasonal shift in runoff pattern that increased vulnerability to winter floods and summer droughts. Increase in extreme cold season precipitation and rain-on-snow events were also responsible for higher frequency of winter floods, which was reflected in an increase in the 95th percentile of extreme daily runoff.

There were distinct differences between the two basins studied. In particular, in the CRB, the suite of changes described above was driven mainly by the warming signal. In the SSJ basin, which is a warmer basin, impacts on water resources were also dependent on changes in precipitation that more often fell in the form of rain in both the control and future climate. As a result, changes in runoff in the SSJ basin responded more directly to precipitation changes.

Climate induced changes in snowpack and runoff will have important impacts on managing water resources for flood control, hydropower production, and irrigation supply in both basins. The situation is further complicated by the potentially reduced soil moisture that may increase irrigation demand and the potential for wild fires during summer.

Our estimation of these effects was based on climate change scenarios that were driven mainly by temperature rather than precipitation changes, especially in the CRB. Given that temperature changes are more certain than precipitation changes, and that the PCM projected temperature changes are on the low end compared with projections based on other climate models (e.g., Mote et al. 1999; Barnett et al. 2001; Cubasch et al. 2001; Miller et al. 2002), our estimated impacts on water resources and agriculture could be small in comparison to other studies. Still the potential impacts and implications for resource management in the future are worthy of further study.

How uncertain are these projections of climate change impacts? This study investigated this issue in part by using ensemble simulations of a GCM and an RCM. If climate signals were estimated from 20-year simulations, our results show that mean monthly climate signals derived from each ensemble simulation were mostly within the standard deviation of the mean monthly signals. If only 10 years of simulation were used, differences among ensemble simulations became larger, especially for spatial distribution of precipitation signals. This suggests a larger ensemble size is necessary for a shorter time.

This study further compared ensemble climate change signals based on three PCM-MM5 downscaling experiments with another experiment that uses different

procedures to generate PCM simulation (historical simulation that starts in 1870 versus initialization with assimilated ocean data of 1995) and downscaling with the RSM model. In all of these experiments, downscaling reduced the warming signal during summer and amplified the precipitation signal of PCM. Although RSM simulations were performed using a perturbation method where large scale fields are nudged towards that of the PCM at all grid points in the domain, differences between PCM and RSM signals were larger than that between PCM and MM5, which suggest that other features, such as physical parameterization differences, were more important. On an annual basis, one cannot distinguish the PCM-RSM signals from those of the PCM-MM5 experiments. On a monthly basis, the signals calculated based on PCM/RSM were more different from PCM/MM5 than individual differences among each pair of ensemble PCM-MM5 experiment. This suggests that physical parameterization differences may be equally or more important than spatial resolution, especially concerning hydroclimate conditions. However differences between the RSM and MM5 simulations were also related to many other differences in the experiment setup. Further investigations of the various factors contributing to uncertainty in model projections of regional climate change will require improved experimental design and coordinated efforts.

To estimate the uncertainty associated with climate change signals, a large suite of experiments is required to encompass all possible differences in the emission scenarios, global climate models, downscaling techniques, and experimental details such as initialization of the atmosphere-ocean GCMs and ways to generate ensembles of GCM and downscaled simulations. When ensemble simulation is applied to downscaling, such a technique may include multiple simulations using one model driven by ensemble global

simulations, use of multiple regional models, and use of ensemble global simulations based on multiple global models. These techniques need to be further explored to provide estimates of uncertainty in climate change signals.

Last, our study, which is based on ensembles of 20-year global and regional simulations, suggests that there is little difference between the signal-to-noise ratios at the regional and global scales (Figure 16). Although climate change signals were generally amplified at the regional scales mainly because of orographic effects, increases in climate variability (or noise) also displayed similar spatial characteristics. This suggests that it may not be necessary to increase the ensemble size to increase the signal-to-noise ratio for climate detection at the regional scales. Similarly, the elevated warming signals in mountainous regions do not necessarily imply an increased signal-to-noise ratio (hence earlier detection) because of enhanced variability. Clearly, more work is required on regional climate predictability to establish the validity of these conclusions.

Acknowledgments

Funding for this study was provided by the U.S. Department of Energy (DOE) Accelerated Climate Prediction Initiative (ACPI). The ACPI Pilot effort was supported largely by the DOE Office of Biological and Environmental Research through numerous contracts and subcontracts to the participants. All MM5 regional climate simulations reported in this study were performed on 64 processors of an IBM-SP3 at the Center for Computational Sciences (CCS), which is supported by the DOE Office of Science, at the Oak Ridge National Laboratory (ORNL). We thank John Drake and his colleagues at

CCS for the excellent computing support. Ying Liu provided technical support in analyzing and managing the large volume of simulation data at PNNL. The PCM simulations were supported by the ACPI and performed at the ORNL CCS and the DOE National Energy Research Scientific Computing Center (NERSC). Pacific Northwest National Laboratory is operated for the U.S. Department of Energy by Battelle Memorial Institute under Contract DE-AC06-76RLO 1830.

References

Barnett, T.P., Pierce, D.W., and Schnur, R.: 2001, "Detection of Anthropogenic Climate Change in the World's Oceans", *Science*, **292**, 270-274.

Cayan, D.R., Redmond, K.T., and Riddle, L.G.: 1999, "ENSO and Hydrologic Extremes in the Western United States", *Journal of Climate*, **12**, 2881-2893.

Cubasch, U., Meehl, G.A., Boer, G.J., Stouffer, R.J., Dix, M., Noda, A., Senior, C.A., Raper, S., Yap, K.S.: 2001, "Chapter 9: Projections of Future Climate Change", Climate *Change 2001: The Scientific Basis. Intergovernmental Panel on Climate Change*, Cambridge University Press, 881pp.

Dai, A., Washington, W.M., and Meehl, G.A.: 2002, "The ACPI Climate Change Simulations", *Climatic Change*, submitted.

Dai, A., Meehl, G.A., Washington, W.M., Wigley, T.M.L., and Arblaster, J.A.: 2001a, "Ensemble Simulation of 21st Century Climate Changes: Business As Usual vs. CO2 Stabilization", *Bull. Am. Met. Soc*., **82**, 2377-2388.

Dai, A., Wigley, T.M.L., Boville, B.A., Kiehl, J.T., and Buja, L.E.: 2001b, "Climates of the 20th and 21st Centuries Simulated by the NCAR Climate System Model", *Journal Climate*, **14**, 485-519.

Daly, C., Neilson, R.P, and Phillips, D.L.: 1994, "A Statistical-Topographic Model For Mapping Climatological Precipitation Over Mountainous Terrain," *Journal of Applied Meteorolog*y **33**, 140-158.

Department of Energy: 1998, *ACPI: The Accelerated Climate Prediction Initiative*. Pacific Northwest National Laboratory, Department of Energy, Germantown, MD, 30pp.

Dickinson, R.E., Kennedy, P.J., Henderson-Sellers, A., and Wilson, M.: 1986, "Biosphere-Atmosphere Transfer Scheme (BATS) for the NCAR Community Climate Model", NCAR Tech. Note, NCAR/TN-275+STR, Natl. Cent. for Atmos. Res., Boulder, Colo.

Gershunov, A., and Barnett, T.P.: 1998, "ENSO Influence on Intraseasonal Extreme Rainfall and Temperature Frequencies in the Contiguous United States: Observations and Model Results," *Journal of Climate*, **11**, 1575-1586.

Giorgi, F., Hurrell, J.W., Marinucci, M.R., and Beniston, M.: 1997, "Elevation Dependency of the Surface Climate Signal: A Model Study," *Journal of Climate*, **10**, 288-296.

Giorgi, F., Hewitson, B., Christensen, J., Hulme, M., Von Storch, H., Whetton, P., Jones, R., Mearns, L., Fu, C.: 2001, "Regional Climate Information – Evaluation and Projections," Climate *Change 2001: The Scientific Basis. Intergovernmental Panel on Climate Change*, Cambridge University Press, 881pp.

Giorgi, F., Mearns, L.O., Shields, C., McDaniel, L.: 1998, "Regional Nested Model Simulations of Present Day and 2xCO2 Climate Over the Central Plains of the U.S.," *Clim. Change*, **40**, 457–493.

Grell, G., Dudhia, J., and Stauffer, D.R.: 1993, "A Description of the Fifth Generation Penn State/NCAR Mesoscale Model (MM5)," *NCAR Tech. Note., NCAR/TN-398+IA*, Nat. Cent. for Atmos. Res., Boulder, CO.

Hamlet, A.F., and Lettenmaier, D.P.: 1999, “Effects of Climate Change on Hydrology and Water Resources in the Columbia River Basin,” *Am. Water Res. Assoc*., **35**, **(6)**, 1597-1623.

Hong, S.-Y., Leetmaa, A.: 1999, “An Evaluation of the NCEP RSM for Regional Climate Modeling”, *Journal of Climate*, **12**, 592-609.

IPCC: 2001, *Climate Change 2001 – The Scientific Basis*. Cambridge University Press, 881pp.

Jones, R.G., Murphy, J.M., Noguer, M., Keen, A.B.,: 1997, “Simulation of Climate Change Over Europe Using a Nested Regional Climate Model. II: Comparison of Driving and Regional Model Responses to a Doubling of Carbon Dioxide,” *Quart. J. R.. Met. Soc*., **123**, 265–292.

Juang, H.-M., Kanamitsu, M.: 1994: “The NMC nested regional spectral model”, *Monthly Weather Review*, **122**, 3-26.

Kim, J.: 2001, “A Nested Modeling Study of Elevation-Dependent Climate Change Signals in California Induced by Increased Atmospheric CO2,” *Geophysical Research Letters*, **28(15)**, 2951.

Laprise R., Caya, D., Giguère, M., Bergeron, G., Côte, H., Blanchet, J.-P., Boer, G.J., McFarlane, N.A.: 1998, “Climate and Climate Change in Western Canada as Simulated by the Canadian Regional Climate Model,” *Atmosphere-Ocean*, **36**, 119–167

Leung, L.R., Qian, Y., and Bian, X.: 2002a, “Hydroclimate of the Western United States Based on Observations and Regional Climate Simulation of 1981-2000. Part I: Seasonal Statistics,” *Journal of Climate*, submitted.

Leung, L.R., Qian, Y., and Bian, X., and Hunt, A.: 2002b, "Hydroclimate of the Western United States Based on Observations and Regional Climate Simulation of 1981-2000. Part II: Mesoscale ENSO Anomalies," *Journal of Climate*, submitted.

Leung, L.R., Qian, Y., Han, J., and Roads, J.O.: 2002c, "Intercomparison of Global Reanalyses and Regional Simulations of Cold Season Water Budgets in the Western U.S.," *Journal of Hydrometeorology*, submitted.

Leung, L.R., and Ghan, S.: 1999a, "Pacific Northwest Climate Sensitivity Simulated by a Regional Climate Model Driven by a GCM. Part I: Control Simulations," *Journal of Climate* **12**, 2010-2030.

Leung, L.R., and Ghan, S.: 1999b, "Pacific Northwest Climate Sensitivity Simulated by a Regional Climate Model Driven by a GCM. Part II: 2xCO_2 Simulations," *Journal of Climate* **12**, 2031-2053.

Leung, L.R., and Wigmosta, M.S.: 1999, "Potential Climate Change Impacts on Mountain Watersheds in the Pacific Northwest," *J. Amer. Water Resour. Assoc.*, **35(6)**, 1463-1471.

Mantua, N.J., Hare, S.R., Zhang, U., Wallace, J.M., and Francis, R.C.: 1997, "A Pacific Interdecadal Climate Oscillation with Impacts on Salmon Production," *Bull. Am. Met. Soc*., **78**, 1069-1079.

Maurer, E.P., O'Donnell, G.M., Lettenmaier, D.P., and Roads, J.O.: 2001, "Evaluation of the Land Surface Water Budget in NCEP/NCAR and NCEP/DOE Reanalyses Using an Off-Line Hydrologic Model," *Journal of Geophysical Research* **106**, 17,841-17,862.

Miller, N.L., Gutowski, W.J., Kim, J., and Strem, E.: 2002, "Assessing California Streamflow for Present Day and 2040 to 2049 Climate Scenarios," *Journal of Hydrometeorology*, in press.

Mote, P., Canning, D., Fluharty, D., Francis, R., Franklin, J., Hamlet, A., Hershman, M., Holmberg, M., Gray-Ideker, K., Keeton, W.S., Lettenmaier, D., Leung, R., Mantua, N., Miles, E., Noble, B., Parandvash, H., Peterson, D.W., Snover, A., Willard, S.: 1999, *Impacts of Climate Variability and Change, Pacific Northwest*, National Atmospheric and Oceanic Administration, Office of Global Programs, and JISAO/SMA Climate Impacts Group, Seattle, WA. 110 pp.

National Assessment Report: 2000, *Water: The Potential Consequences of Climate Variability and Change for the Water Resources of the United States*, a report of the National Water Assessment Group for the U.S. Global Change Research Program. 151 pp.

Pierce, D.W., Barnett, T.P., Tokmakian, R., Semtner, A., Maltrud, M., Lysne, J., and Craig, A.: 2002, "The ACPI Demonstration Project Element 1: Initializing the Coupled Model From Observed Conditions," *Climatic Change*, submitted.

Roads, J.O., and Chen, S.-C.: 2000, "Surface Water and Energy Budgets in the NCEP Regional Spectral Model", *JGR-Atmospheres*, **105**, 29539-29550.

Roads, J.O., Chen, S.-C., Kanamitsu, M.,: 2002, "US Regional Climate Simulations and Seasonal Forecasts, *J. Geophys. Res*., accepted.

Whetton P.H., Katzfey, J.J., Hennesey, K.J., Wu, X., McGregor, J.L., Nguyen, K.: 2001, "Using Regional Climate Models to Develop Fine Resolution Scenarios of Climate Change: An Example for Victoria, Australia," *Clim. Res*., **16**, 181-201.

Washington, W.M., Weatherly, J.W., Meehl, G.A., Semtner, A.J., Bettge, T.W., Craig, A.P., Strand, W.G. Jr., Arblaster, J., Wayland, V.B., James, R., Zhang, Y.: 2000, "Parallel Climate Model (PCM) Control and Transient Simulations," *Climate Dynamics*, **16**, 755-774.

TABLE CAPTION

Table 1. A summary of global and regional climate models and characteristics of simulations used in this study.

Table 2. Changes in seasonal mean and 95th percentile precipitation (P), mean and 95th percentile runoff (R), precipitation intensity and frequency, snowfall, amount of rainfall in rain-on-snow events, and frequency of rain-on-snow events based on ensemble average of MM5 simulations for each season (December – February, DJF; March – May, MAM; June – August, JJA; and September – November, SON) in the CRB and SSJ basins.

Table 3. Annual and seasonal mean changes in precipitation (P), temperature (T), snow water equivalent (S), runoff (R), sensible heat flux (SH), latent heat flux (LH), net shortwave radiation (SW), and net longwave radiation (LW) based on ensemble mean PCM and MM5 simulations of future (2040-2060) and control (1995-2015) climate averaged over the Columbia River Basin (CRB) and Sacramento-San Joaquin (SSJ) Basin.

FIGURE CAPTION

Figure 1. Nested domain at 40 km spatial resolution used in the regional climate model. Shown in the figure are the grid locations of the PCM (large dots) and MM5 (small dots), contours of elevation defined in the MM5, outlines of the Columbia River Basin (CRB) and Sacramento-San Joaquin (SSJ) Basin boundaries, and locations of six regions used in the analysis of surface temperature of Figures 7 and 8. Each region occupied 4 RCM grid cells.

Figure 2. Annual mean temperature (^{o}C) and precipitation (mm/day) averaged over the CRB and SSJ basin for the PCM historical simulation (1975-1995, solid lines) and control simulation (1995-2045, dash lines) respectively.

Figure 3. Spatial distribution of seasonal mean surface temperature (^{o}C) based on the PCM (top panel) and RCM (middle panel) control simulations and observations (bottom) for summer (left) and winter (right).

Figure 4. Similar to Figure 3, but for seasonal mean precipitation in mm/day.

Figure 5. Basin averaged monthly mean surface temperature (^{o}C) and precipitation (mm/day) based on the PCM and RCM control simulations and observations.

Figure 6. Spatial distribution of seasonal mean surface temperature changes (^{o}C) based on differences between the PCM (top panel) and RCM (bottom panel) ensemble mean of the 2040-2060 climate conditions and the control simulation (1995-2015) for summer (JJA) and winter (DJF). Contours are for temperature change at an interval of 0.4^{o}C. Areas with temperature change above the 0.95 confidence level are shaded in grey.

Figure 7. Frequency distributions of daily mean temperature in six regions shown in Figure 1 based on the RCM control and future climate simulations. Blue and red correspond to winter (DJF) and summer (JJA) values respectively, with solid curves representing the control simulation and dash curves the ensemble future simulations. The regions are located in (1) Cascades, (2) Columbia Basin, (3) Northern Rockies, (4) Sierra, (5) Intermountain West, and (6) Southwest respectively.

Figure 8. Similar to Figure 7, but for frequency distribution of diurnal temperature range (DTR).

Figure 9. Similar to Figure 6, but for precipitation changes in mm/day. Contour interval is 0.3 mm/day.

Figure 10. Changes in 95th percentile daily precipitation (mm) for summer and winter.

Figure 11. Absolute (left) and percentage (right) changes in annual mean snowpack (mm) by mid-century compared with the control simulation based on the PCM (top) and MM5 (bottom) simulations.

Figure 12. Changes in monthly mean surface water budget averaged over the CRB and SSJ basin. Shown in the figure are changes in precipitation (P), snowpack accumulation rate (SP), runoff (R), soil moisture accumulation rate (SM), and evapotranspiration (ET) in mm/day.

Figure 13. Changes in monthly mean surface energy budget averaged over the CRB and SSJ basin. Shown in the figure are changes in sensible (SH) and latent (LH) heat fluxes and net shortwave (SW) and longwave (LW) radiation in W/m^2.

Figure 14. Basin mean annual temperature (^oC) and precipitation (mm/day) based on three ensemble PCM simulations for 1995-2100 in the CRB and SSJ basin.

Figure 15. Basin mean monthly temperature and precipitation signals calculated as the difference between the 20-year (2040-2060) mean monthly temperature or precipitation based on each ensemble simulation and 20-year (1995-2015) of the control simulation averaged over the CRB and SSJ basin. Also shown in the figure are vertical bars showing the standard deviations of the mean monthly signals of each ensemble simulation.

Figure 16. Signal-to-noise ratio for precipitation (left) and temperature (right) based on the PCM (upper) and MM5 (lower) simulations.

Figure 17. Spatial distribution of seasonal mean surface temperature (^{o}C) (upper) and precipitation (lower) changes (mm/day) based on differences between the RSM simulated 2040-2050 and 1986-1996 climate conditions for summer (JJA) and winter (DJF). Contours are at intervals of 0.4^{o}C and 0.3 mm/day for temperature and precipitation changes respectively. Areas with changes above the 0.95 confidence level are shaded in grey.

Figure 18. Basin mean monthly temperature and precipitation signals based on each PCM and downscaled simulation for 2040-2050. Curves shown in black are for PCM simulations and those shown in grey are for downscaled simulations. Each pair of black and grey curves having the same pattern corresponds to each set of three ensemble simulations performed with PCM (PCM 1, 2, and 3) and MM5 and one set of simulation performed with PCM (PCM 4) and RSM. Table 1 listed the differences between the MM5 and RSM numerical experiments.

Table 1.

Model	**PCM**			**MM5**		**RSM**	
Model Resolution	T42; 18 vertical levels			Nested 120km/40km; 23 vertical levels		50 km; 28 vertical levels	
Type of Simulation	Control	Historical	Climate Change	Control	Climate Change	Control	Climate Change
Simulation Period	1995-2075	1870-2100	1995-2100	1995-2015	2040-2060	1986-1996	2040-2050
Number of Simulations/ Case Number	1 (B06.45)	3 (B06.30, B06.31, B06.32)	3 (B06.44, B06.46, B06.47)	1	3	1	1
Greenhouse Gases and Aerosol Forcing	1995 CO_2 and sulfate aerosol concentrations	Historical CO_2 and aerosol from 1870-1996; business as usual scenario from 1997 to 2100	Business as usual scenario from 1995 to 2100	1995 CO_2 concentration (358 ppmv)	2040-2060 CO_2 concentration (~ 505 ppmv)	1986-1996 CO_2 concentration (~)	2040-2050 CO_2 concentration (~)
Initial Conditions	Assimilated 1995 ocean condition (Pierce et al. 2002)	Three different initial atmospheric conditions for 1870	Assimilated 1995 ocean condition and 3 different initial atmospheric conditions for 1995	Based on PCM control simulation on July 1995	Based on each of 3 ensemble PCM climate change simulations on July 2040	Based on one PCM historical simulation on June 1986	Based on one PCM historical simulation on June 2040
Boundary Conditions				Based on PCM control simulation	Based on each of 3 ensemble PCM climate change simulations	Based on one PCM historical simulation	Based on one PCM historical simulation

Table 2.

Basins	**CRB**				**SSJ**			
Seasons	**SON**	**DJF**	**MAM**	**JJA**	**SON**	**DJF**	**MAM**	**JJA**
Mean P (mm/day)	-0.19 (-7%)	-0.02 (-1%)	-0.01 (0%)	-0.20 (-20%)	0.09 (7%)	-0.24 (-4%)	-0.26 (-10%)	-0.08 (-27%)
95% P (mm/day)	0.11 (1%)	1.05 (6%)	0.20 (2%)	-1.10 (-12%)	2.36 (8%)	3.97 (9%)	-1.19 (-4%)	-3.33 (-32%)
Mean R (mm/day)	-0.01 (-20%)	0.02 (40%)	-0.05 (-28%)	0.00 (0%)	0.02 (67%)	0.02 (6%)	-0.03 (-20%)	0.00 (0%)
95% R (mm/day)	-0.07 (-9%)	0.08 (11%)	-0.59 (-31%)	-0.10 (-31%)	0.63 (43%)	0.61 (14%)	-0.18 (-7%)	-0.20 (-53%)
P Intensity (mm/day)	0.13 (2%)	0.34 (7%)	0.12 (4%)	-0.24 (-10%)	0.97 (14%)	1.11 (9%)	-0.22 (-3%)	-0.73 (-24%)
P Frequency (%)	-4.78 (-10%)	-4.95 (-7%)	-2.67 (-4%)	-4.95 (-13%)	-0.97 (-5%)	-5.43 (-12%)	-2.55 (-7%)	-1.92 (-19%)
Snowfall (mm/day)	-0.20 (-21%)	-0.34 (-13%)	-0.24 (-19%)	-0.02 (-67%)	-0.03 (-30%)	-0.45 (-34%)	-0.26 (-37%)	0.00 (0%)
Rain-On-Snow Amount (mm/day)	-0.06 (-11%)	0.12 (17%)	0.03 (14%)	-0.01 (-50%)	-0.01 (-13%)	-0.15 (-17%)	-0.05 (-24%)	0.00 (0%)
Rain-On-Snow Frequency (%)	-0.35 (-10%)	0.49 (10%)	0.11 (4%)	-0.2 (-74%)	-0.08 (-20%)	-0.36 (-14%)	-0.16 (-15%)	-0.02 (-100%)

Table 3.

		CRB			SSJ		
	Model	**JJA**	**DJF**	**Annual**	**JJA**	**DJF**	**Annual**
P (mm/day)	**MM5**	-0.20	-0.02	-0.10	-0.08	-0.24	-0.12
	PCM	-0.09	0.00	-0.04	-0.04	-0.35	-0.08
T (^oC)	**MM5**	1.59	1.50	1.56	1.26	1.54	1.37
	PCM	1.78	1.83	1.65	1.32	1.31	1.34
S (mm)	**MM5**	-0.07	-23.55	-15.41	0.00	-7.49	-4.10
	PCM	-0.08	-18.60	-9.45	0.00	-0.67	-0.21
R (mm/day)	**MM5**	-0.12	0.22	-0.08	-0.03	0.12	-0.09
	PCM	-0.11	-0.08	-0.07	-0.28	-0.06	-0.15
SH (W/m^2)	**MM5**	5.52	-1.29	1.01	4.45	-0.33	1.13
	PCM	6.85	1.07	2.00	1.43	-0.68	-0.37
LH (W/m^2)	**MM5**	-0.62	-1.41	-0.81	-1.97	-0.39	-0.40
	PCM	-1.34	-0.01	1.00	1.57	1.92	2.88
SW (W/m^2)	**MM5**	-0.25	0.43	0.68	0.32	0.41	0.04
	PCM	8.43	3.32	4.19	3.04	2.39	2.51
LW (W/m^2)	**MM5**	0.12	-0.89	-0.70	0.06	-0.91	-0.10
	PCM	4.05	1.21	1.63	-0.03	1.45	0.60

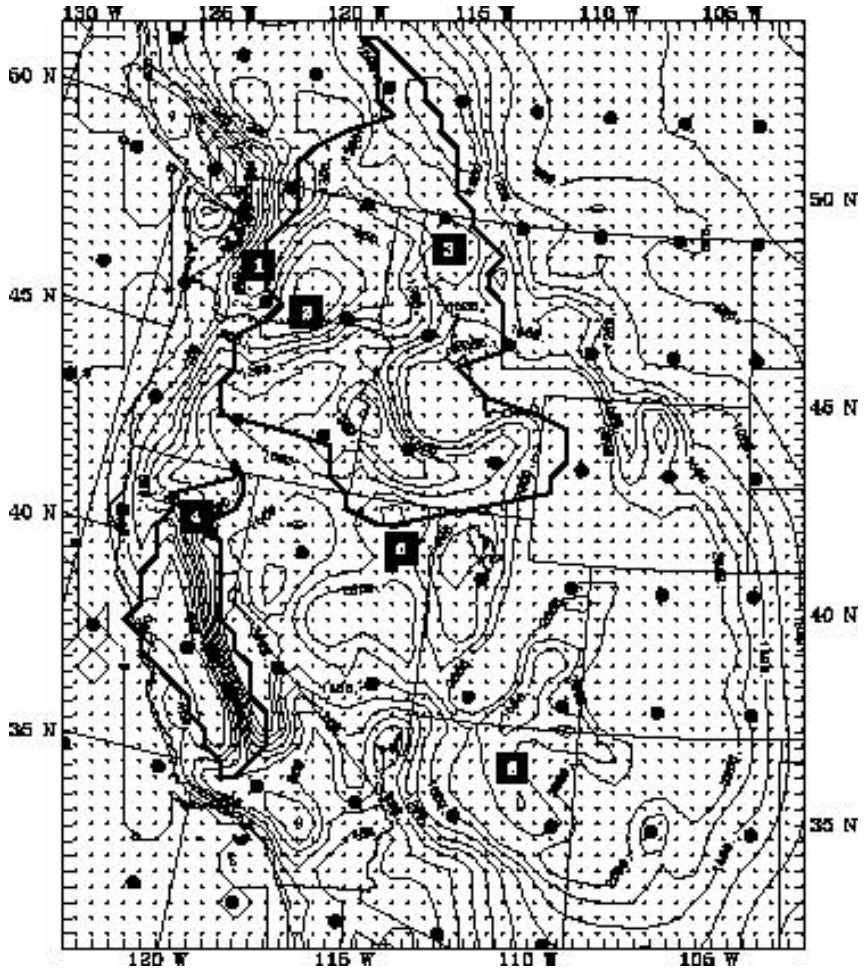
130 W
125 W
120 W
115 W
110 W
105 W
50 N
45 N
40 N
35 N
120 W
115 W
110 W
105 W

Figure 1

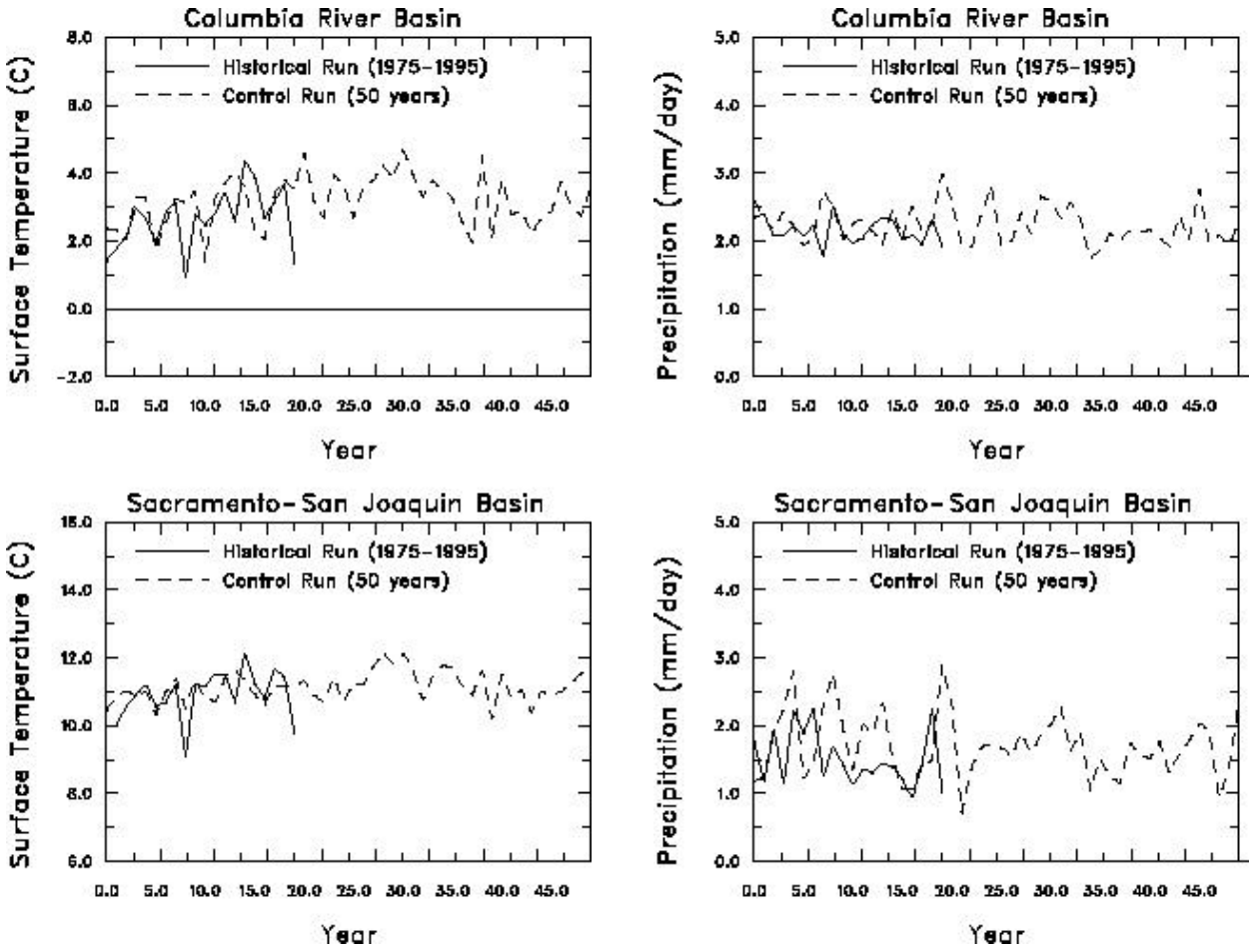
Columbia River Basin
Historical Run (1975-1995)
Control Run (50 years)
Surface Temperature (C)
Year
Columbia River Basin
Historical Run (1975-1995)
Control Run (50 years)
Precipitation (mm/day)
Year
Sacramento-San Joaquin Basin
Historical Run (1975-1995)
Control Run (50 years)
Surface Temperature (C)
Year
Sacramento-San Joaquin Basin
Historical Run (1975-1995)
Control Run (50 years)
Precipitation (mm/day)
Year

Figure 2

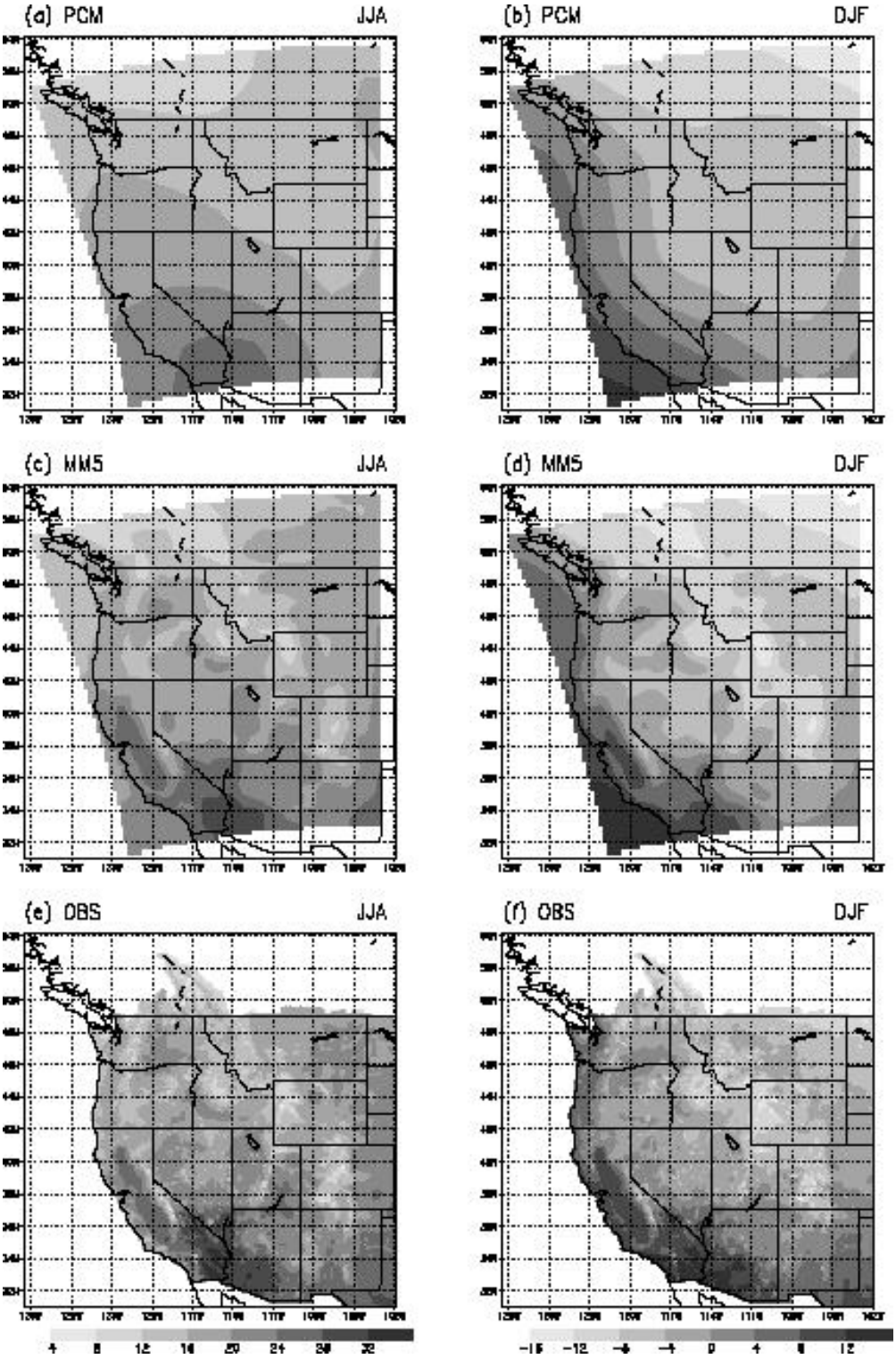

Figure 3

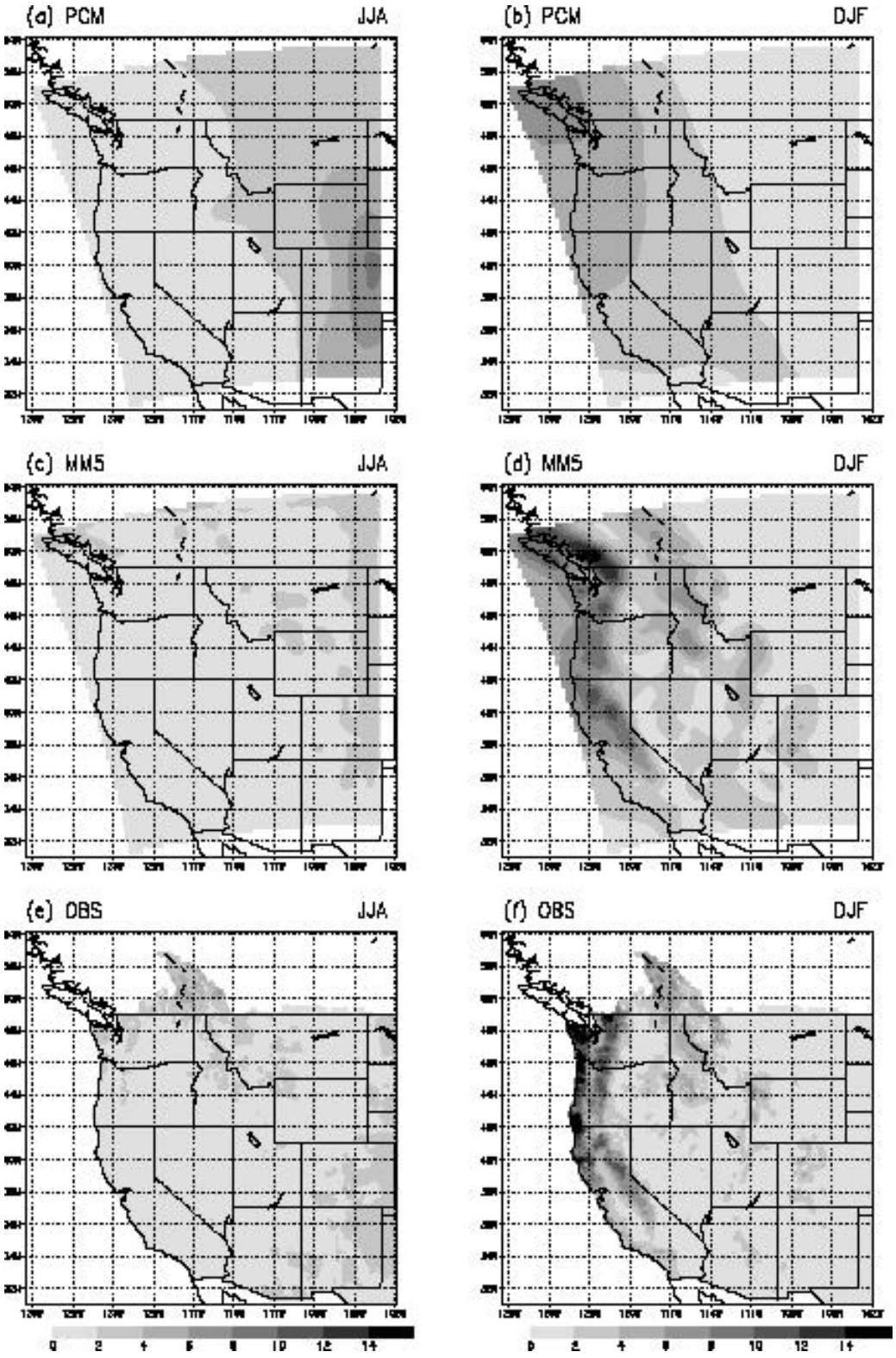
(a) PCM
JJA
(b) PCM
DJF
(c) MM5
JJA
(d) MM5
DJF
(e) OBS
JJA
(f) OBS
DJF
0 2 4 6 8 10 12 14
0 2 4 6 8 10 12 14

Figure 4

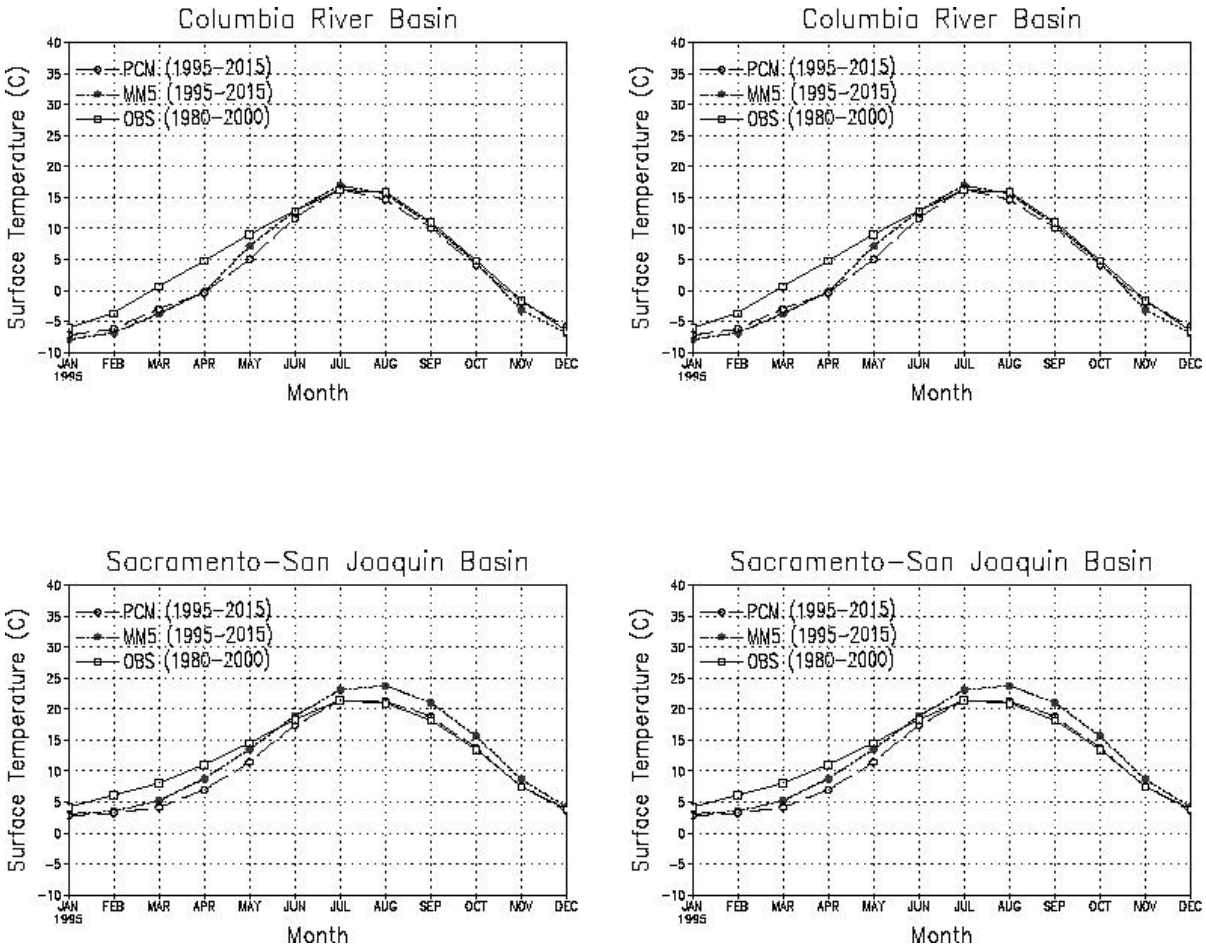
Columbia River Basin
PCM (1995-2015)
MM5 (1995-2015)
OBS (1980-2000)
Surface Temperature (C)
Month
JAN 1995
FEB
MAR
APR
MAY
JUN
JUL
AUG
SEP
OCT
NOV
DEC
Columbia River Basin
PCM (1995-2015)
MM5 (1995-2015)
OBS (1980-2000)
Surface Temperature (C)
Month
Sacramento-San Joaquin Basin
PCM (1995-2015)
MM5 (1995-2015)
OBS (1980-2000)
Surface Temperature (C)
Month
Sacramento-San Joaquin Basin
PCM (1995-2015)
MM5 (1995-2015)
OBS (1980-2000)
Surface Temperature (C)
Month

Figure 6

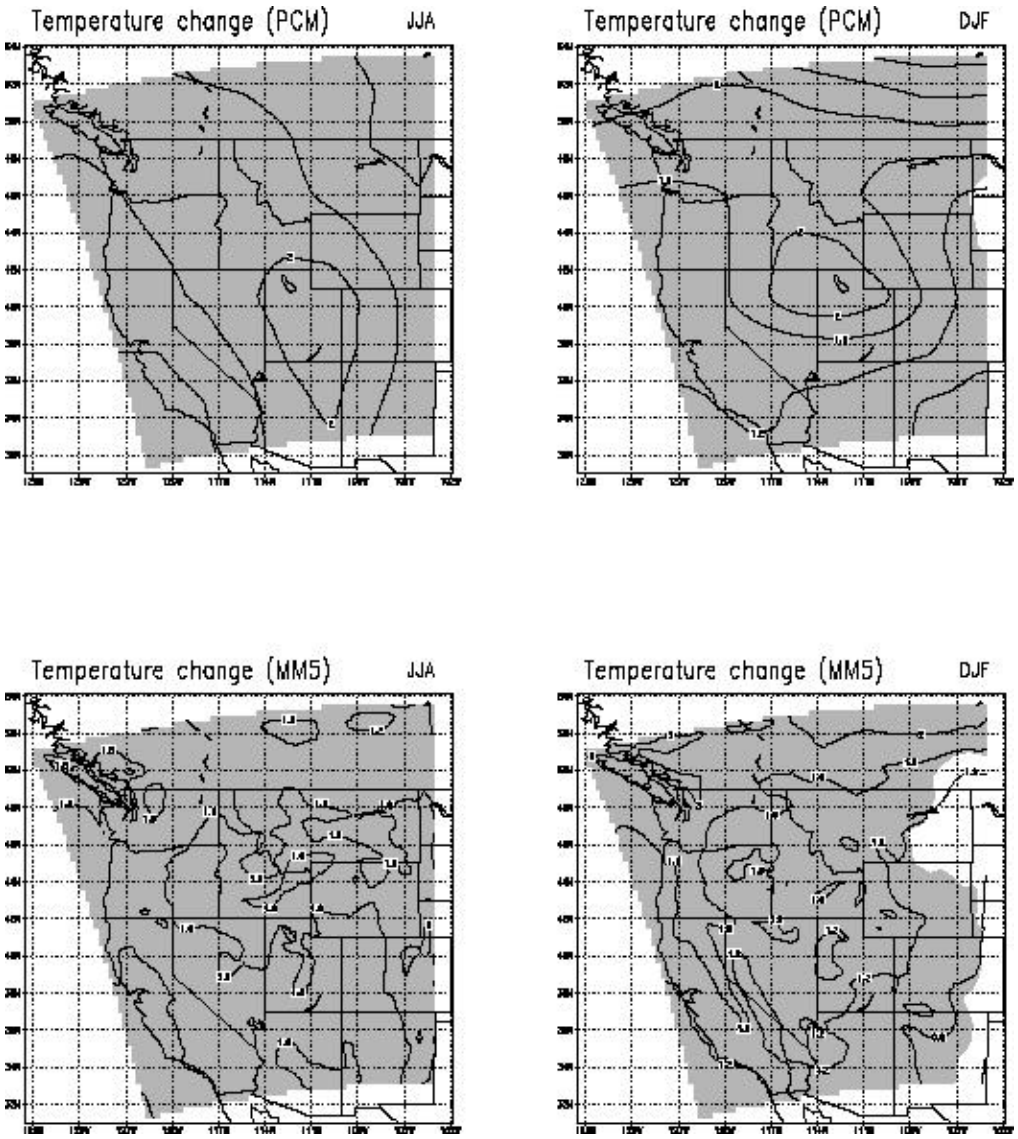
Temperature change (PCM)
JJA
Temperature change (PCM)
DJF
Temperature change (MM5)
JJA
Temperature change (MM5)
DJF

Figure 6

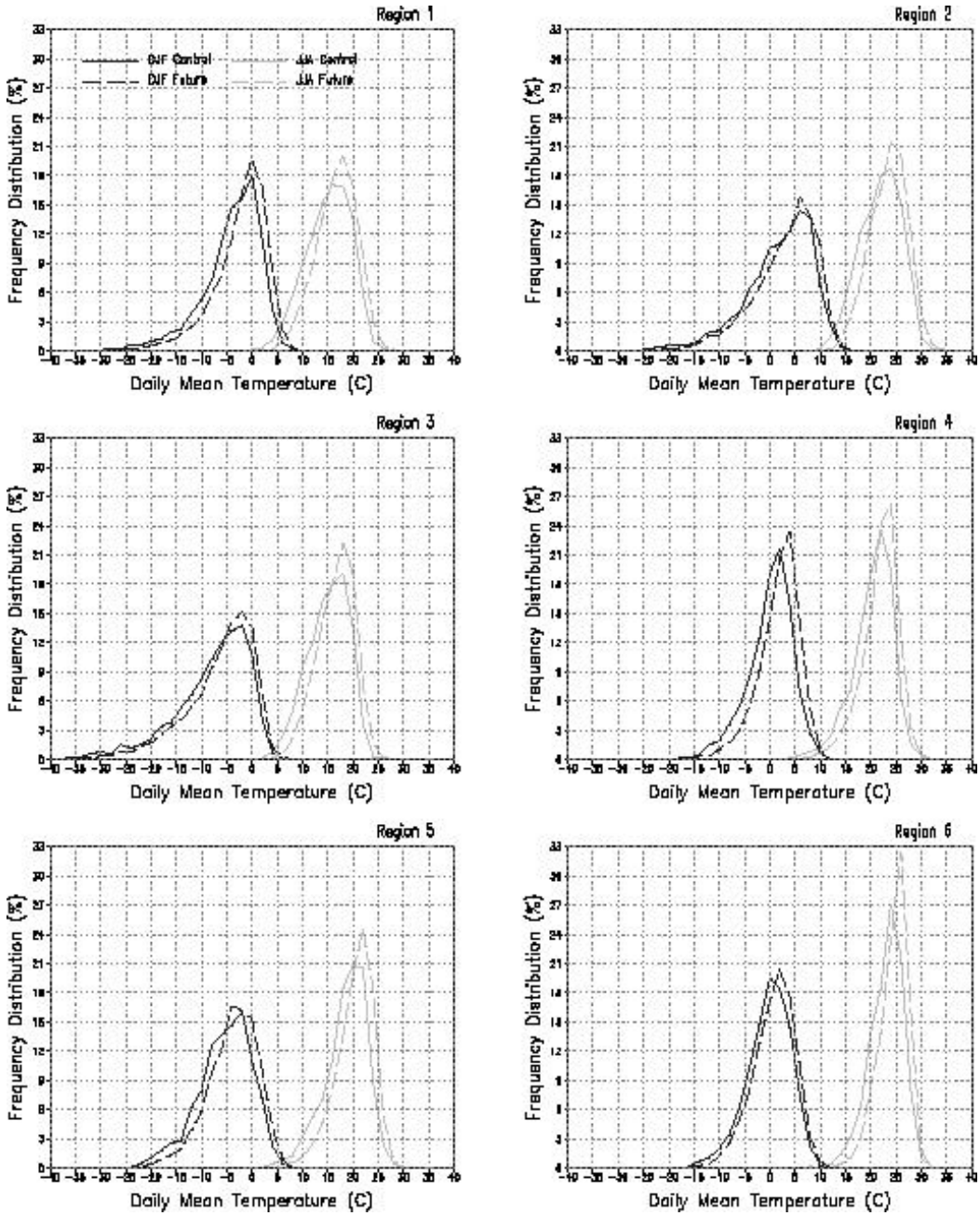
Region 1
Region 2
Region 3
Region 4
Region 5
Region 6
DJF Control
DJF Future
JJA Control
JJA Future
Frequency Distribution (%)
Daily Mean Temperature (C)

Figure 7

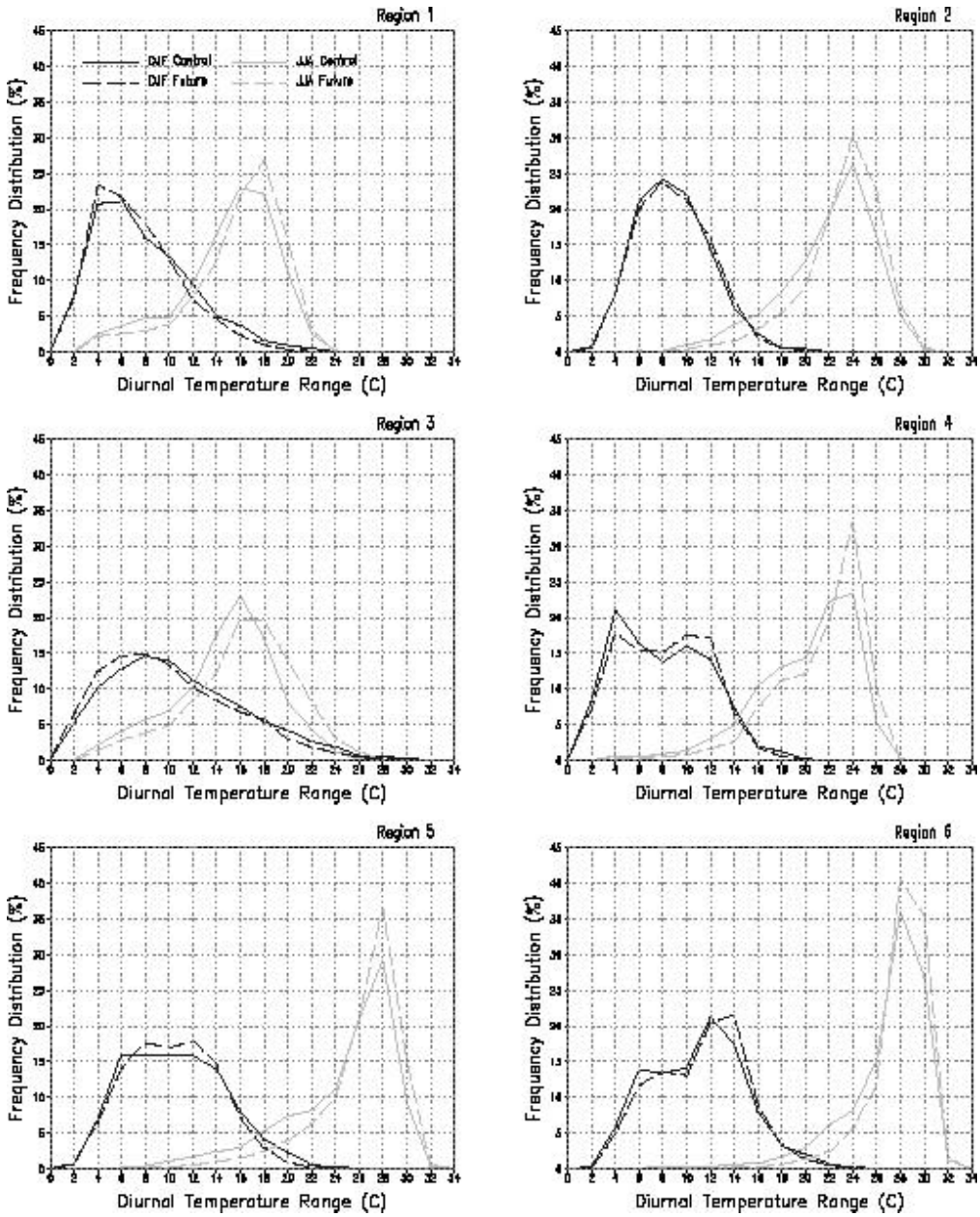
Region 1
Region 2
Region 3
Region 4
Region 5
Region 6
DJF Control
DJF Future
JJA Control
JJA Future
Frequency Distribution (%)
Diurnal Temperature Range (C)

Figure 8

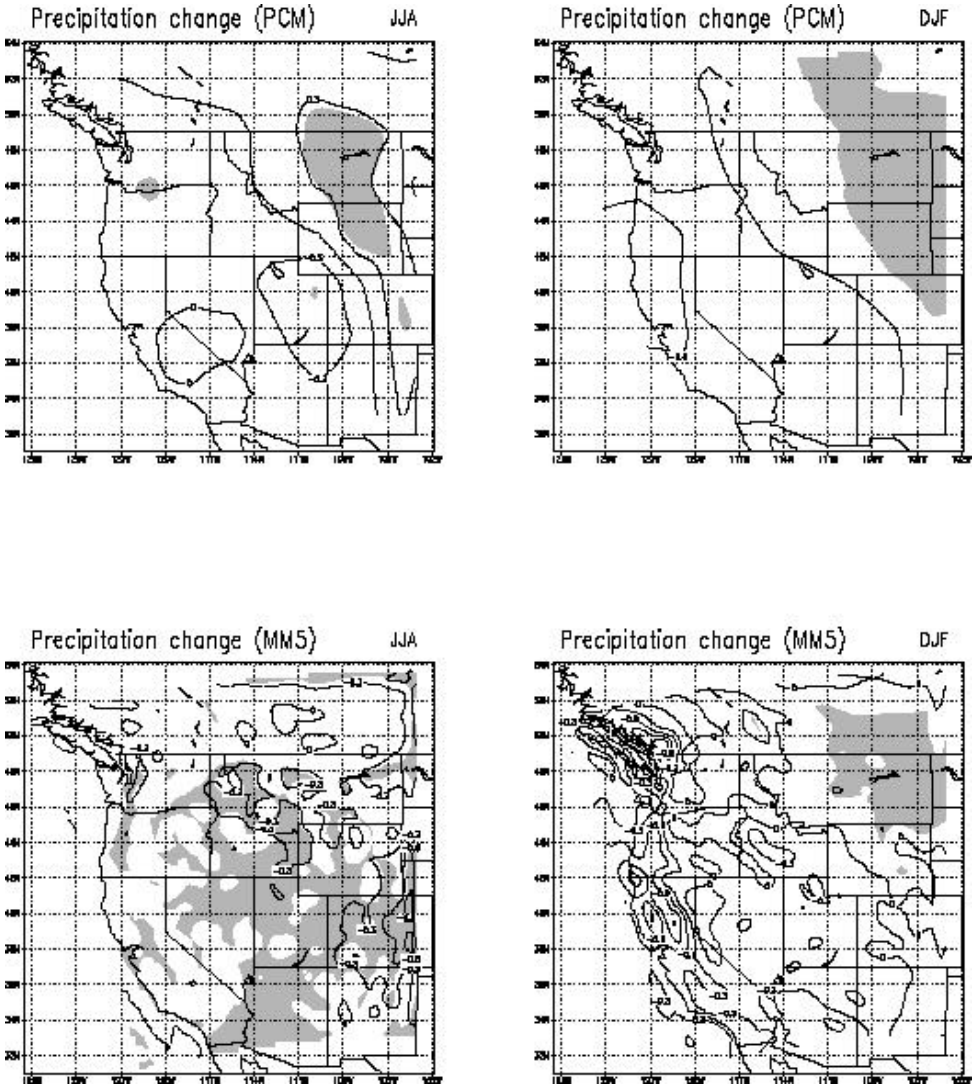
Precipitation change (PCM)
JJA
Precipitation change (PCM)
DJF
Precipitation change (MM5)
JJA
Precipitation change (MM5)
DJF

Figure 9

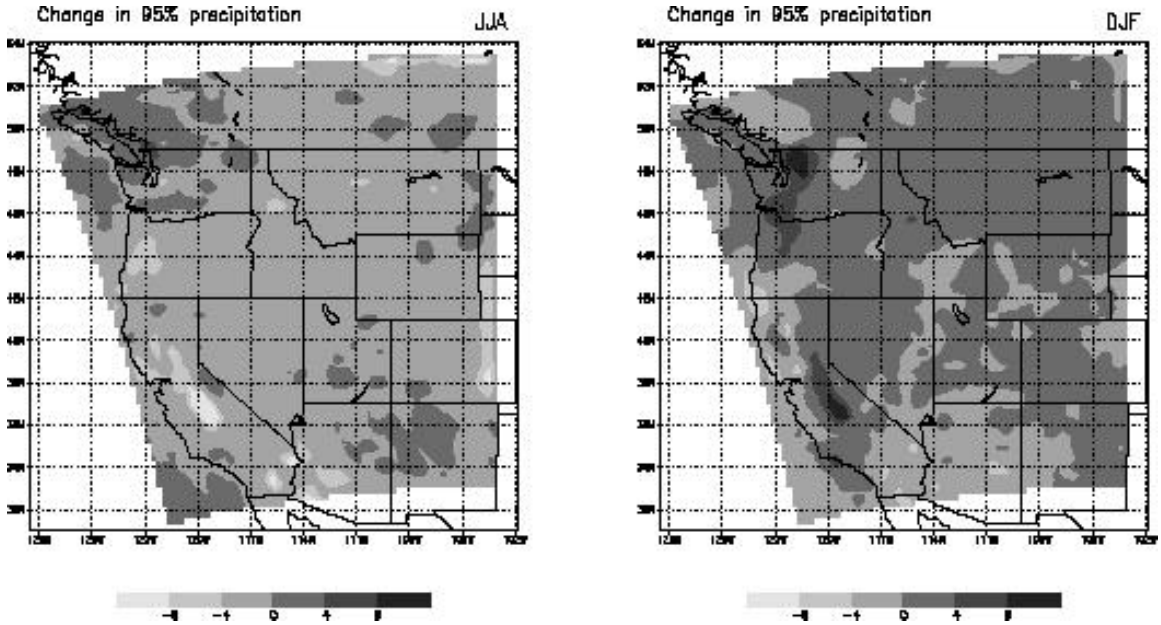
Change in 95% precipitation
JJA
Change in 95% precipitation
DJF

Figure 10

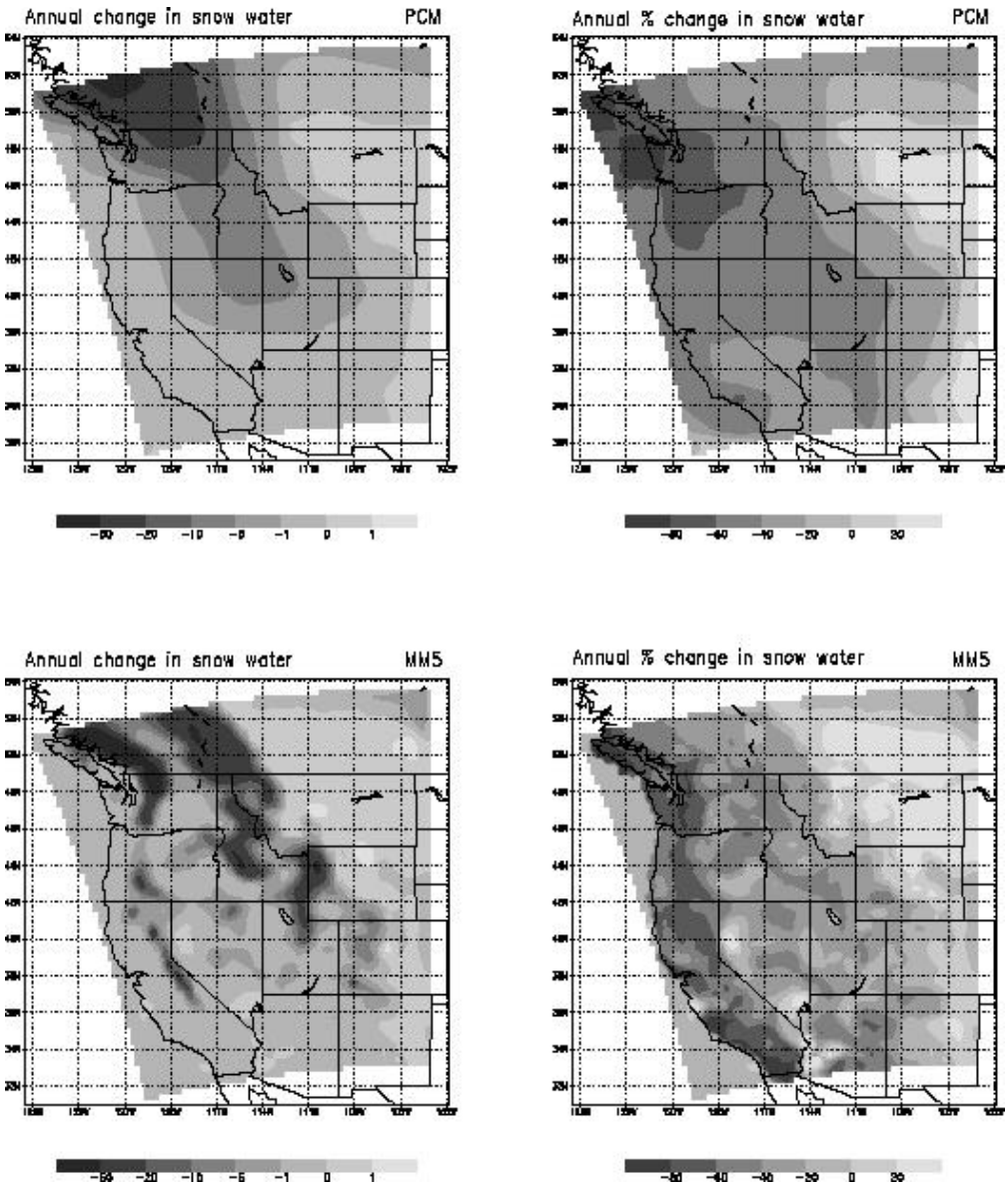
Annual change in snow water
PCM
Annual % change in snow water
PCM
Annual change in snow water
MM5
Annual % change in snow water
MM5

Figure 11

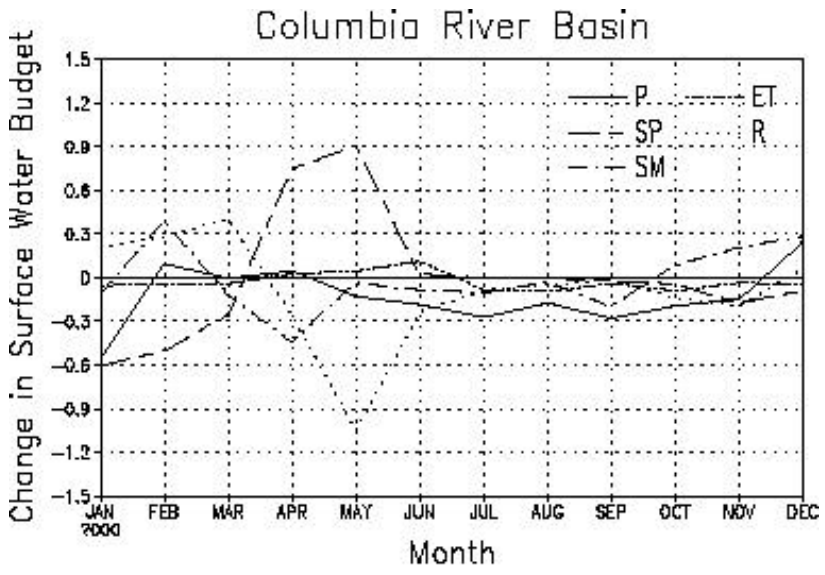
Columbia River Basin
Change in Surface Water Budget
1.5
1.2
0.9
0.6
0.3
0
-0.3
-0.6
-0.9
-1.2
-1.5
P
ET
SP
R
SM
JAN 2000
FEB
MAR
APR
MAY
JUN
JUL
AUG
SEP
OCT
NOV
DEC
Month

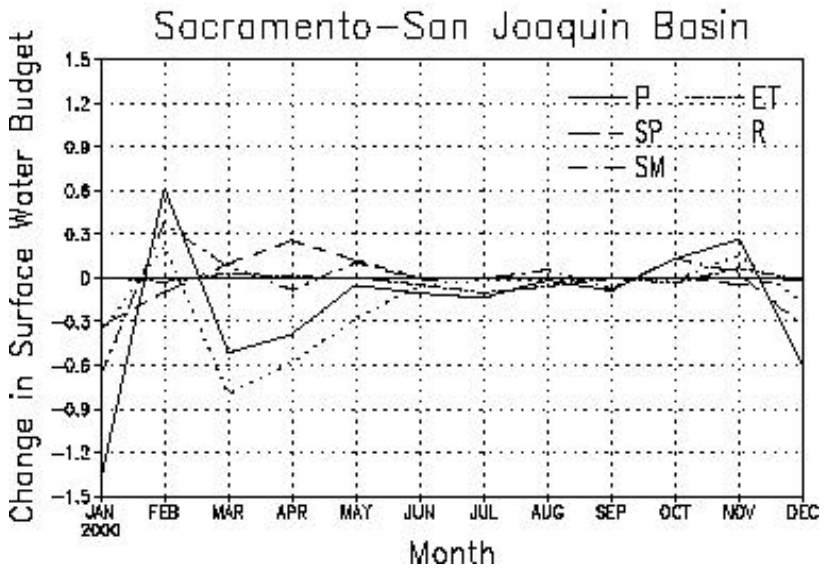
Sacramento-San Joaquin Basin
Change in Surface Water Budget
1.5
1.2
0.9
0.6
0.3
0
-0.3
-0.6
-0.9
-1.2
-1.5
P
ET
SP
R
SM
JAN 2000
FEB
MAR
APR
MAY
JUN
JUL
AUG
SEP
OCT
NOV
DEC
Month

Figure 12

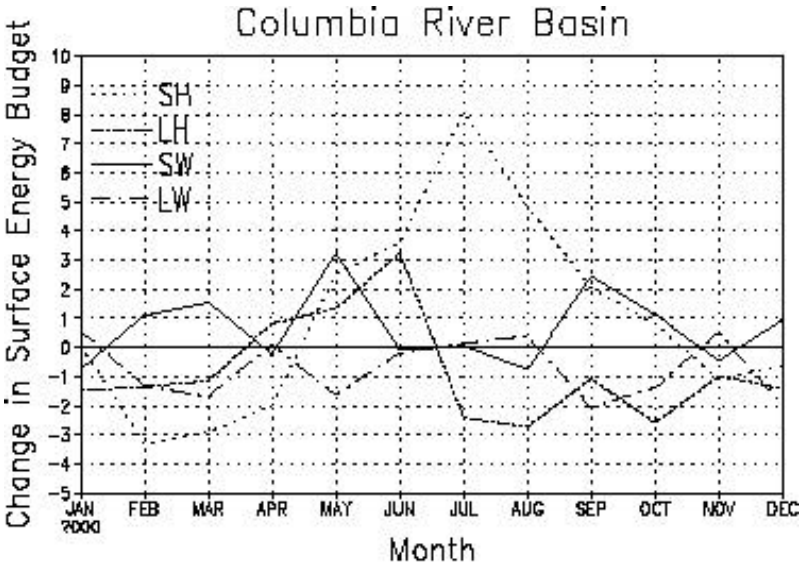
Columbia River Basin
Change in Surface Energy Budget
SH
LH
SW
LW
10
9
8
7
6
5
4
3
2
1
0
-1
-2
-3
-4
-5
JAN 2000
FEB
MAR
APR
MAY
JUN
JUL
AUG
SEP
OCT
NOV
DEC
Month

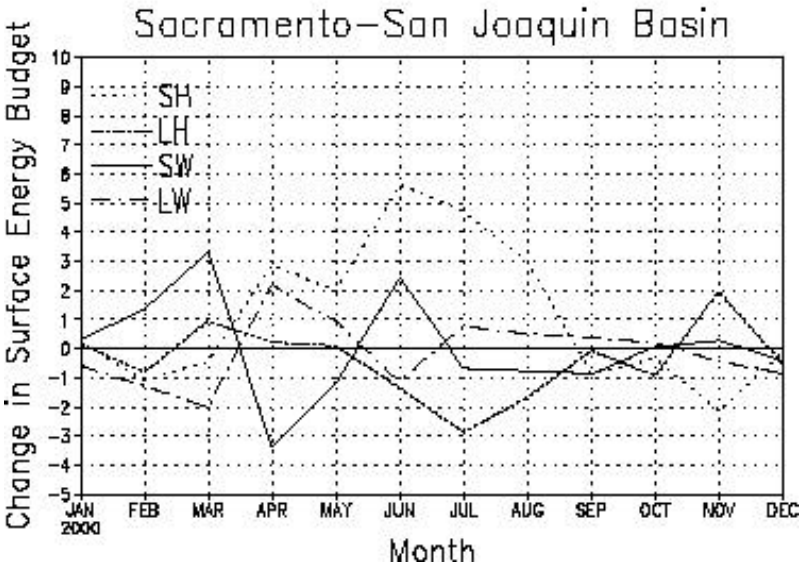
Sacramento-San Joaquin Basin
Change in Surface Energy Budget
SH
LH
SW
LW
10
9
8
7
6
5
4
3
2
1
0
-1
-2
-3
-4
-5
JAN 2000
FEB
MAR
APR
MAY
JUN
JUL
AUG
SEP
OCT
NOV
DEC
Month

Figure 13

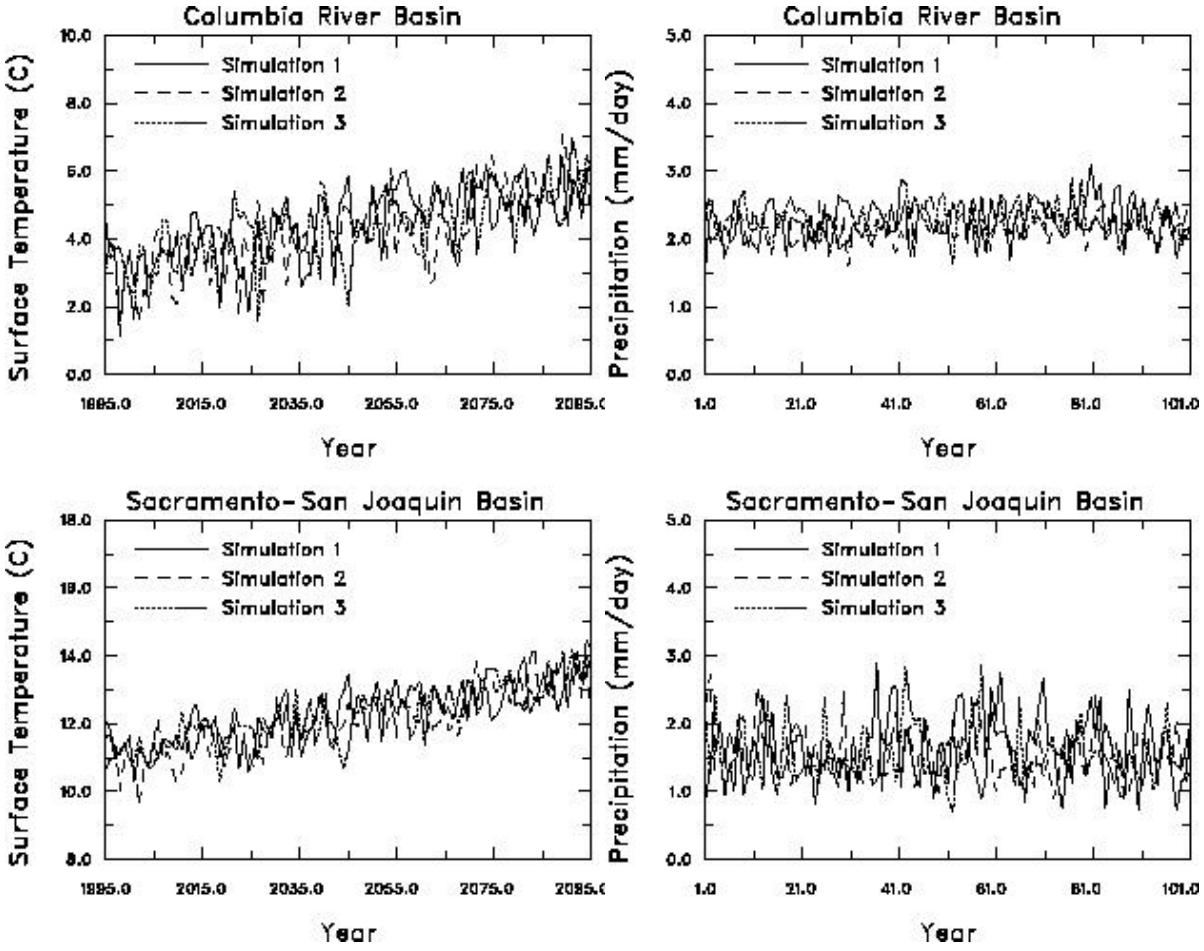
Columbia River Basin
Simulation 1
Simulation 2
Simulation 3
Surface Temperature (C)
Year
Columbia River Basin
Precipitation (mm/day)
Year
Sacramento-San Joaquin Basin
Surface Temperature (C)
Year
Sacramento-San Joaquin Basin
Precipitation (mm/day)
Year

Figure 14

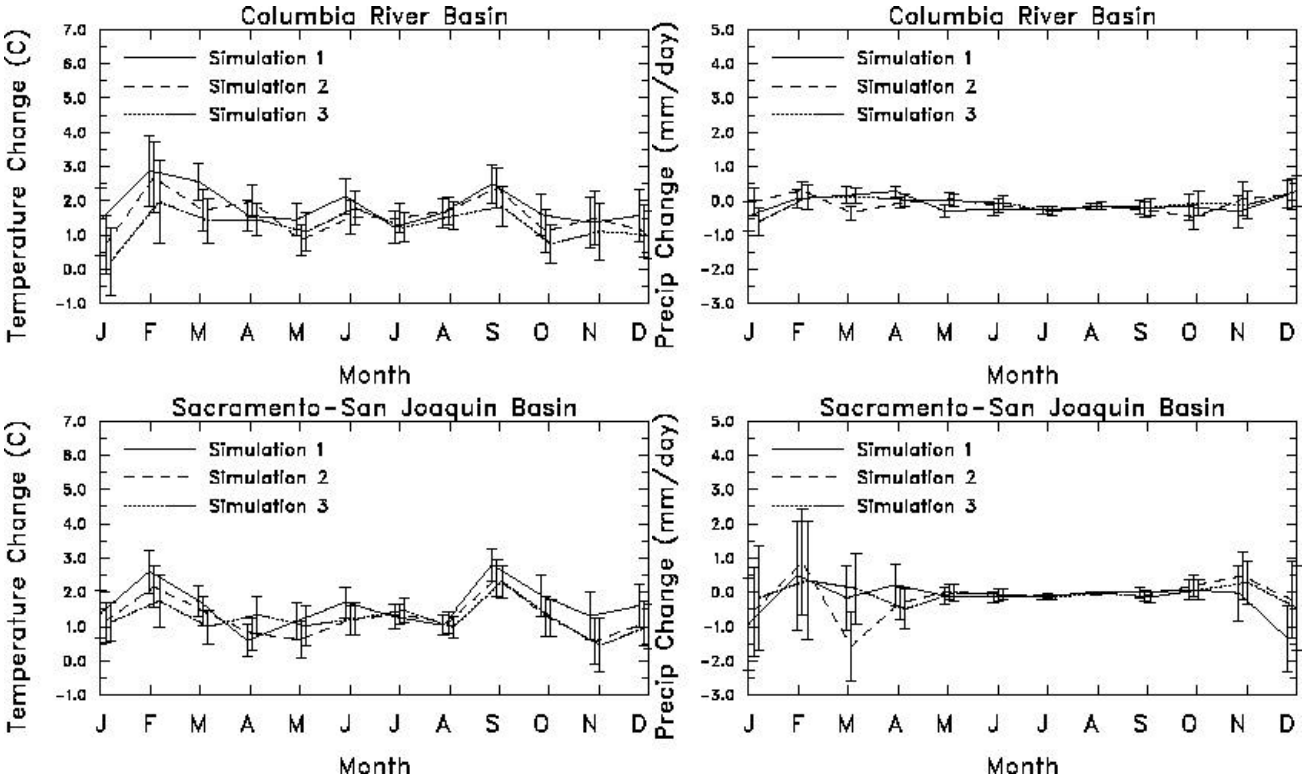
Columbia River Basin
Sacramento-San Joaquin Basin
Simulation 1
Simulation 2
Simulation 3
Temperature Change (C)
Precip Change (mm/day)
Month
J F M A M J J A S O N D

Figure 15

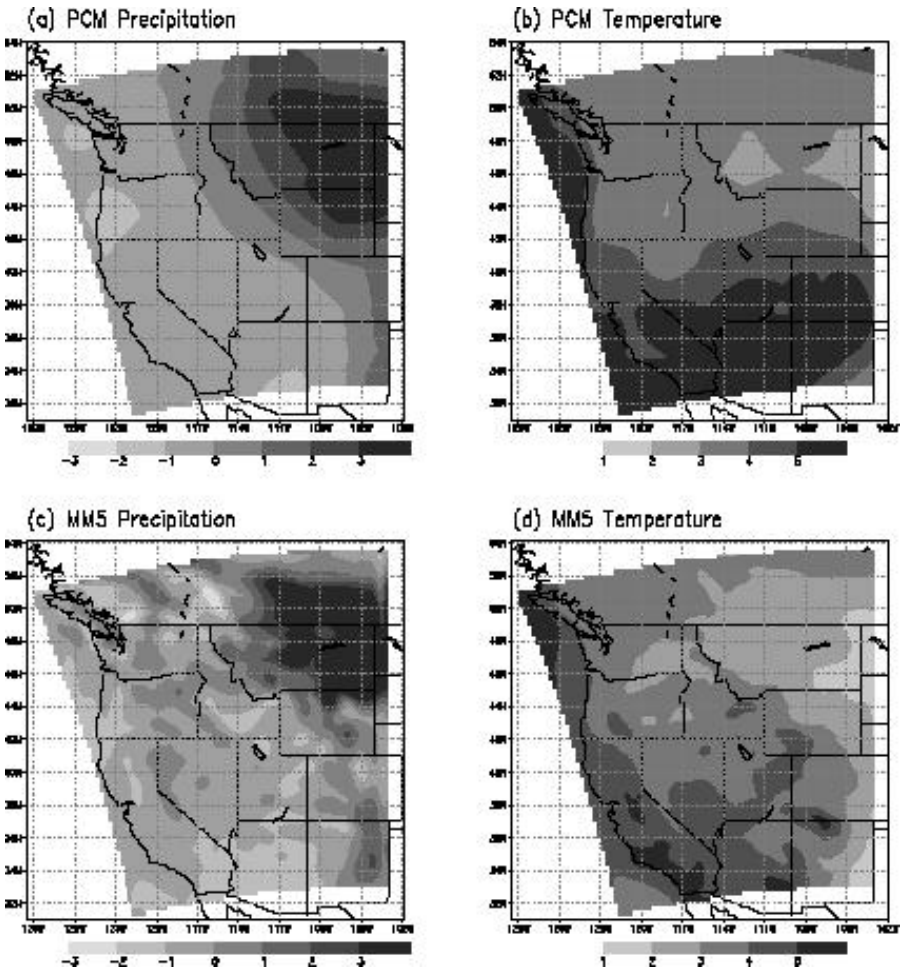
(a) PCM Precipitation
(b) PCM Temperature
(c) MM5 Precipitation
(d) MM5 Temperature

Figure 16

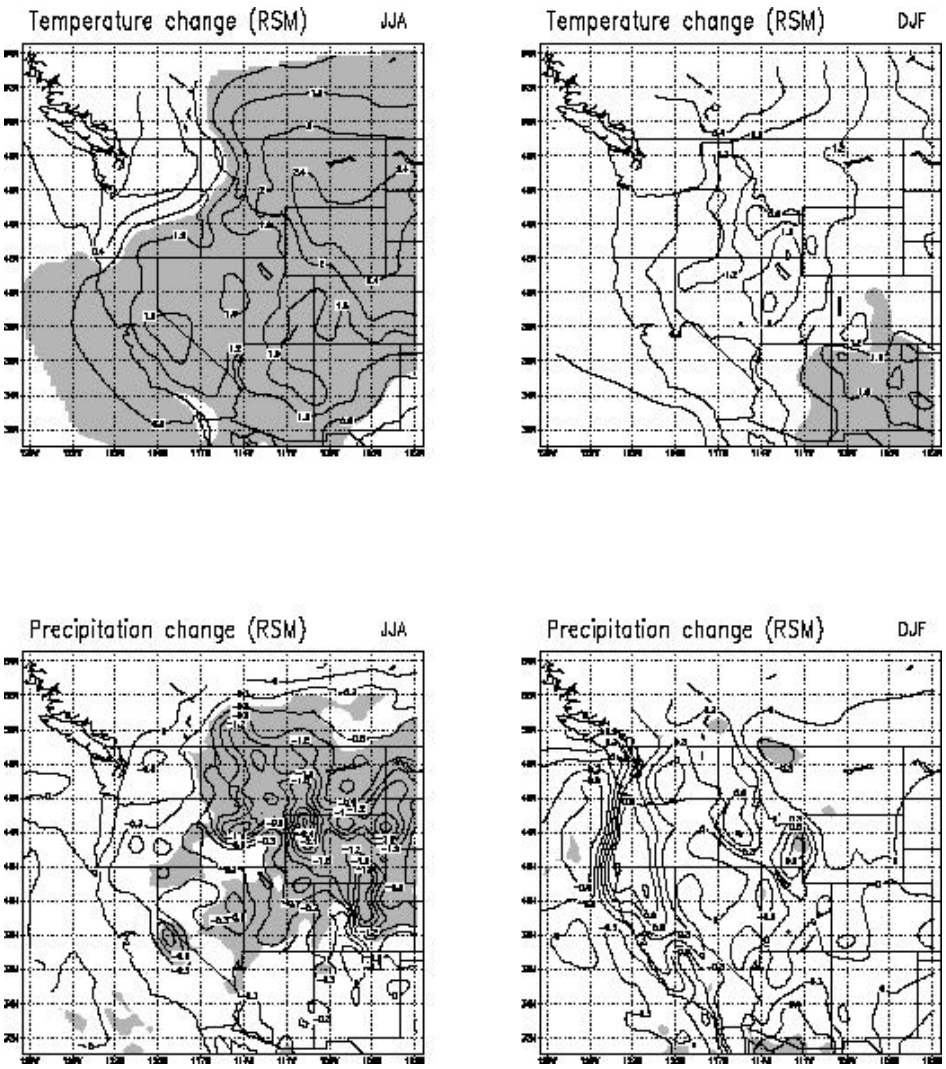
Temperature change (RSM)
JJA
Temperature change (RSM)
DJF
Precipitation change (RSM)
JJA
Precipitation change (RSM)
DJF

Figure 17

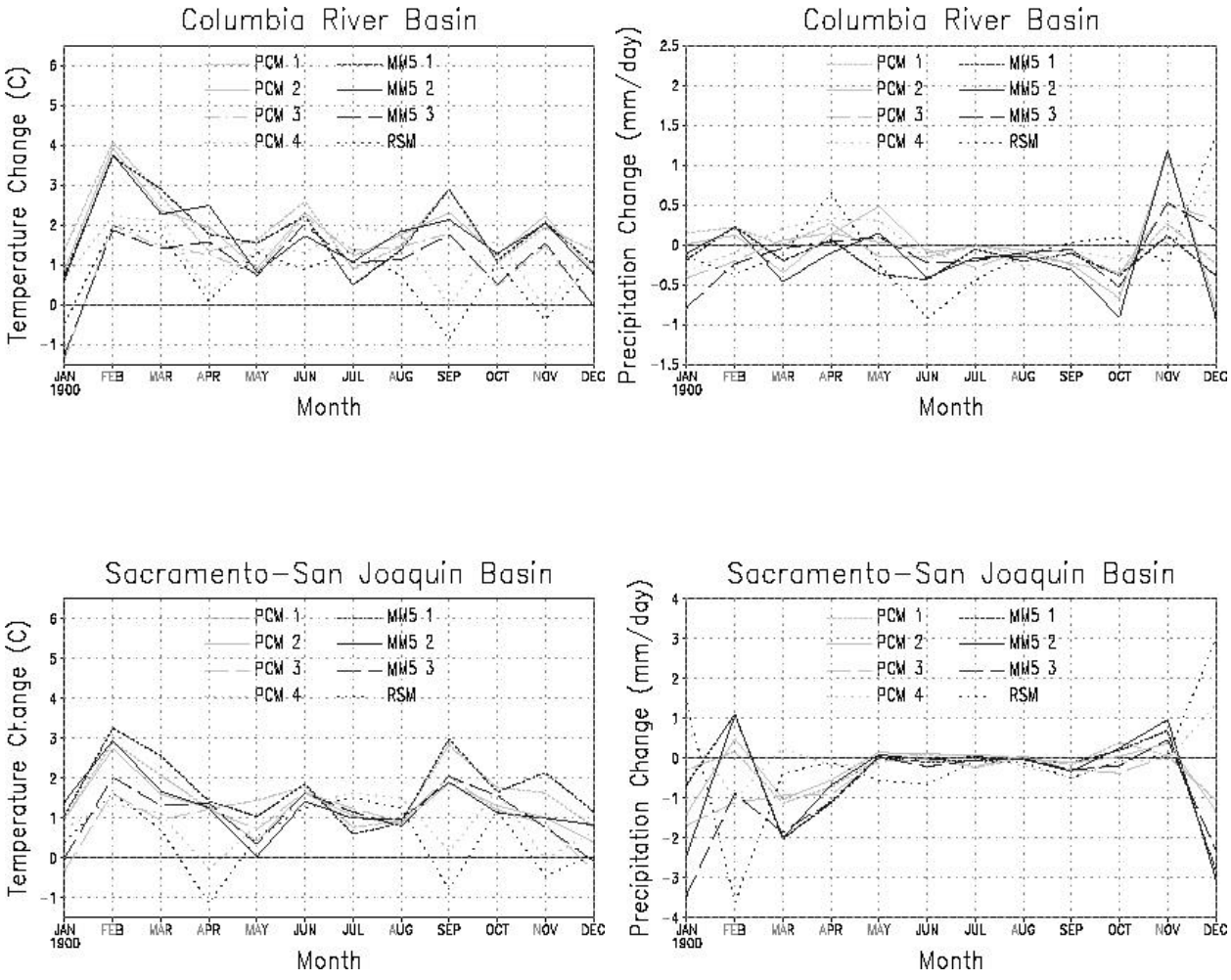
Columbia River Basin
Temperature Change (C)
Month
Columbia River Basin
Precipitation Change (mm/day)
Month
Sacramento–San Joaquin Basin
Temperature Change (C)
Month
Sacramento–San Joaquin Basin
Precipitation Change (mm/day)
Month
PCM 1
PCM 2
PCM 3
PCM 4
MM5 1
MM5 2
MM5 3
RSM
JAN 1900
FEB
MAR
APR
MAY
JUN
JUL
AUG
SEP
OCT
NOV
DEC

Figure 18